The Astrophysical Journal, 665:187–208, 2007 August 10

FORMATION OF $z \sim 6$ QUASARS FROM HIERARCHICAL GALAXY MERGERS

Yuexing Li,[1] Lars Hernquist,[1] Brant Robertson,[1,2,3] Thomas J. Cox,[1] Philip F. Hopkins,[1] Volker Springel,[4] Liang Gao,[5] Tiziana Di Matteo,[6] Andrew R. Zentner,[2] Adrian Jenkins,[5] and Naoki Yoshida[7]
Received 2006 August 9; accepted 2007 April 9

ABSTRACT

The discovery of luminous quasars at redshift $z \sim 6$ indicates the presence of supermassive black holes (SMBHs) of mass $\sim 10^9\ M_\odot$ when the universe was less than 1 billion years old. This finding presents several challenges for theoretical models because whether such massive objects can form so early in the ΛCDM cosmology, the leading theory for cosmic structure formation, is an open question. Furthermore, whether the formation process requires exotic physics such as super-Eddington accretion remains undecided. Here we present the first multiscale simulations that, together with a self-regulated model for the SMBH growth, produce a luminous quasar at $z \sim 6.5$ in the ΛCDM paradigm. We follow the hierarchical assembly history of the most massive halo in a $\sim 3\ \mathrm{Gpc}^3$ volume and find that this halo of $\sim 8 \times 10^{12}\ M_\odot$ forming at $z \sim 6.5$ after several major mergers is able to reproduce a number of observed properties of SDSS J1148+5251, the most distant quasar detected at $z = 6.42$ (Fan et al. 2003). Moreover, the SMBHs grow through gas accretion below the Eddington limit in a self-regulated manner owing to feedback. We find that the progenitors experience vigorous star formation (up to $10^4\ M_\odot\ \mathrm{yr}^{-1}$) preceding the major quasar phase such that the stellar mass of the quasar host reaches $10^{12}\ M_\odot$ at $z \sim 6.5$, consistent with observations of significant metal enrichment in SDSS J1148+5251. The merger remnant thus obeys a similar $M_{\rm BH}$-$M_{\rm bulge}$ scaling relation observed locally as a consequence of coeval growth and evolution of the SMBH and its host galaxy. Our results provide a viable formation mechanism for $z \sim 6$ quasars in the standard ΛCDM cosmology and demonstrate a common, merger-driven origin for the rarest quasars and the fundamental $M_{\rm BH}$-$M_{\rm bulge}$ correlation in a hierarchical universe.

Subject headings: black hole physics — cosmology: theory — early universe — galaxies: active — galaxies: evolution — galaxies: formation — galaxies: high-redshift — galaxies: ISM — galaxies: starburst — methods: numerical — quasars: general — quasars: individual (SDSS J1148+5251)

1. INTRODUCTION

Quasars rank among the most luminous objects in the universe and are believed to be powered by SMBHs (e.g., Salpeter 1964; Lynden-Bell 1969). They constrain the formation and evolution of galaxies and SMBHs throughout cosmic time. The similarity between the cosmic star formation history (e.g., Madau et al. 1996; Bunker et al. 2004; Bouwens et al. 2004) and the evolution of quasar abundances (e.g., Shaver et al. 1996) suggests an intriguing link between galaxy formation and black hole (BH) growth. This is strengthened by tight correlations measured locally between the masses of the BHs and the global properties of the spheroid components of their hosts, such as their luminosities and masses (Magorrian et al. 1998; Marconi & Hunt 2003), light concentration (Graham et al. 2001), and velocity dispersions (Ferrarese & Merritt 2000; Gebhardt et al. 2000; Tremaine et al. 2002).

Distant, highly luminous quasars are important cosmological probes for studying the first generation of galaxies, the star formation history and metal enrichment in the early universe, the growth of the first supermassive black holes (SMBHs), the role of feedback from quasars and BHs in galaxy evolution, and the epoch of reionization. The Sloan Digital Sky Survey (SDSS; York et al. 2000) has contributed significantly to the discovery of high-redshift quasars. Currently, there are over 1000 quasars known at $z \gtrsim 4$ and 12 at $z \gtrsim 6$ (Fan et al. 2001, 2003, 2004, 2006). As reviewed by Fan (2006), quasars at $z \sim 6$ are characterized by (1) a low space density ($\sim 10^{-9}\ \mathrm{Mpc}^{-3}$ comoving); (2) high luminosities (absolute luminosity at rest-frame $M_{1450\,\text{Å}} < -26$), believed to be powered by SMBHs of $\sim 10^9\ M_\odot$; (3) Gunn-Peterson absorption troughs (Gunn & Peterson 1965) in their spectra, which place these quasars at the end of the epoch of reionization (e.g., Fan et al. 2001; Becker et al. 2001; Djorgovski et al. 2001; Lidz et al. 2002; Songaila & Cowie 2002; White et al. 2003; Sokasian et al. 2003); and (4) a lack of evolution in the spectral energy distribution (SED) compared to lower redshift counterparts (e.g., Elvis et al. 1994; Glikman et al. 2006; Richards et al. 2006), which demonstrates the existence of "mature" quasars at early times and comparable metal enrichment in quasars at all cosmic epochs.

The most distant quasar known, SDSS J1148+5251 (hereafter J1148+5251), was discovered by SDSS at $z = 6.42$ (Fan et al. 2003). It is extremely bright optically with $M_{1450\,\text{Å}} = -27.8$, and deep imaging surveys in both optical and radio (Carilli et al. 2004; White et al. 2005; Willott et al. 2005) show no sign of gravitational lensing or other companions at the same redshift in the vicinity. Over the past few years, this quasar has been extensively studied at many wavelengths. Near-infrared (NIR) observations by Willott et al. (2003) and Barth et al. (2003) imply a bolometric luminosity of $L_{\rm bol} \sim 10^{14}\ L_\odot$ powered by accretion onto an SMBH of mass $(1-5) \times 10^9\ M_\odot$. Radio observations by Bertoldi et al. (2003a) and Carilli et al. (2004) suggest that the host is a hyperluminous far-infrared (FIR) galaxy, with $L_{\rm FIR} \sim 10^{13}\ L_\odot$, and these authors estimate a star formation rate (SFR) of $\sim 3 \times 10^3\ M_\odot\ \mathrm{yr}^{-1}$ by assuming that most of the FIR luminosity comes from young

[1] Harvard-Smithsonian Center for Astrophysics, Harvard University, Cambridge, MA 02138; yxli@cfa.harvard.edu.
[2] Kavli Institute for Cosmological Physics, Department of Astronomy and Astrophysics, University of Chicago, Chicago, IL 60637.
[3] Spitzer Fellow.
[4] Max-Planck-Institute for Astrophysics, 85740 Garching, Germany.
[5] Institute for Computational Cosmology, Department of Physics, University of Durham, Durham DH1 3LE, UK.
[6] Department of Physics, Carnegie Mellon University, Pittsburgh, PA 15213.
[7] Department of Physics, Nagoya University, Nagoya, Aichi 464-8602, Japan.

stars. Emission from carbon monoxide (CO) has been detected (Walter et al. 2003, 2004; Bertoldi et al. 2003b) corresponding to a mass of $\sim 2 \times 10^{10}\ M_{\odot}$. Dust has been seen by several groups (e.g., Robson et al. 2004; Bertoldi et al. 2003a; Carilli et al. 2004; Beelen et al. 2006) with an estimated mass of $\sim 5 \times 10^{8}\ M_{\odot}$. In particular, *Spitzer* observations by Charmandaris et al. (2004) and Hines et al. (2006) indicate that the dust is heated by an active galactic nucleus (AGN). Furthermore, the detection of iron by Barth et al. (2003), the carbon fine-structure line [C II] by Maiolino et al. (2005), and excess O I absorption by Becker et al. (2006) indicates near-solar metallicity in the quasar host.

These observations raise many fundamental questions for models of quasar and galaxy formation: Where do such high-redshift, luminous quasars originate? How do they form? What are the mechanisms and physical conditions for SMBH growth? And, do these quasar hosts obey the same SMBH-host correlations as observed in the local universe?

Interpretations of various observations of J1148+5251 have painted a rather conflicting picture for the formation site of the quasar halo and the SMBH-host relationship. The low abundance of these quasars leads to the view that they are hosted by massive halos ($\gtrsim 10^{13}\ M_{\odot}$) in the rarest density peaks of the dark matter distribution (Fan et al. 2003). However, it has been argued, based on the lack of companion galaxies in the field, that this quasar may reside in a much lower mass halo in a less overdense region (Carilli et al. 2004; Willott et al. 2005). Moreover, Walter et al. (2004) suggest, based on the dynamical mass estimate from CO measurements, that J1148+5251 contains a small stellar spheroid and that the SMBH may have largely formed before the host galaxy. However, the detection of metal lines (Walter et al. 2004; Barth et al. 2003; Maiolino et al. 2005), along with dust (Bertoldi et al. 2003a; Carilli et al. 2004; Robson et al. 2004; Charmandaris et al. 2004; Hines et al. 2006; Beelen et al. 2006), indicates that the interstellar medium (ISM) of J1148+5251 was significantly enriched by heavy elements produced through massive star formation at rates of $\sim 10^{3}\ M_{\odot}\ \mathrm{yr}^{-1}$ occurring as early as $z \gtrsim 10$, and that large stellar bulges form before accreting SMBHs undergo luminous quasar activity.

In an expanding universe that is dominated by cold dark matter (CDM) and is accelerated by dark energy, the ΛCDM cosmology, the leading theoretical model for structure formation, assumes that structure grows from weak density fluctuations amplified by gravity, with small objects collapsing first and subsequently merging to form progressively more massive ones, a process known as "hierarchical assembly" (for a review see, e.g., Barkana & Loeb 2001). The formation of galaxies and quasars is therefore determined by the abundance of dark matter halos, i.e., the number density of halos as a function of mass and redshift. The most widely used analytic model for the halo mass function was first developed by Press & Schechter (1974) (hereafter PS), which is based on Gaussian density perturbations, linear gravitational growth, and spherical collapse of dark matter. Using the PS mass functions, Efstathiou & Rees (1988) studied the abundance of rare objects, such as luminous quasars at high redshifts. These authors predicted a sharp "cutoff" of the quasar population at $z \sim 5$. However, while the initial, linear growth of density perturbations can be calculated analytically, the gravitational collapse and subsequent hierarchical buildup of structure is a highly nonlinear process that can be followed only through numerical simulations. It has been shown by previous numerical studies (e.g., Jenkins et al. 2001; Sheth & Tormen 2002; Springel & Hernquist 2003b) and more recently by the state-of-the-art Millennium Simulation by Springel et al. (2005c) that the PS formula underestimates the abundance of high-mass halos by up to an order of magnitude. Therefore, whether or not rare quasars such as J1148+5251 can form in the ΛCDM cosmology remains an open question and an important test of the theory.

To date, only a limited number of analytical or semianalytic models have addressed the early formation of a $10^{9}\ M_{\odot}$ SMBH at $z \sim 6$ (Haiman & Loeb 2001; Haiman 2004; Yoo & Miralda-Escudé 2004; Volonteri & Rees 2005). These approaches use merger trees of dark matter halos generated using the PS theory and assume a BH accretion rate at or above the Eddington limit. However, as discussed above, the PS-based approach may be inaccurate. Moreover, it is not clear whether sufficient physical conditions for such large accretion rates exist in quasar systems as the hydrodynamics of the large-scale gas flow and feedback from BHs have not been incorporated in earlier modeling.

It is believed that the growth of SMBHs is closely linked to galaxy formation (e.g., Magorrian et al. 1998; Ferrarese & Merritt 2000; Gebhardt et al. 2000; Graham et al. 2001; Tremaine et al. 2002; Marconi & Hunt 2003; Haiman 2004; Kazantzidis et al. 2005; Li et al. 2007a) and that the growth is self-regulated by feedback (e.g., Silk & Rees 1998; Haehnelt et al. 1998; Fabian 1999; King 2003; Wyithe & Loeb 2003; Di Matteo et al. 2005; Springel et al. 2005b; Sazonov et al. 2005; Murray et al. 2005; Wyithe & Loeb 2005). Remarkably, self-regulated models with SMBH feedback in the form of thermal energy coupled to the ambient gas have been demonstrated to successfully reproduce many observations of galaxies, including the M_{BH}-σ relation (Di Matteo et al. 2005; Robertson et al. 2006b), galaxy colors (Springel et al. 2005a; Hopkins et al. 2006c), X-ray gas emission (Cox et al. 2006a), elliptical kinematics (Cox et al. 2006b), the fundamental plane (Robertson et al. 2006a), quasar properties (Hopkins et al. 2005a, 2005d), luminosity functions (Hopkins et al. 2005b, 2005c, 2006b), populations (Hopkins et al. 2006a, 2006d, 2007b), and the luminosity function of low-level AGNs (Hopkins & Hernquist 2006). Furthermore, these simulations of binary mergers identify a plausible, merger-driven formation mechanism for massive BHs and luminous quasars (e.g., Di Matteo et al. 2005; Hopkins et al. 2006a; Robertson et al. 2006b).

Here we present a model that accounts for the SMBH growth, quasar activity, and host galaxy properties of the most distant quasar known. In our scenario, the quasar and its host galaxy form in a massive halo that originates from a rare density peak in the standard ΛCDM paradigm, and they grow hierarchically through multiple gas-rich mergers, supporting an average SFR of $\sim 10^{3}\ M_{\odot}\ \mathrm{yr}^{-1}$ that peaks at $z \sim 8.5$. Once the progenitors undergo sufficient dynamical friction to coalesce, the multiple SMBHs from the progenitor galaxies merge and exponentially increase their mass and feedback energy via accretion. At $z \approx 6.5$ when the SMBH mass exceeds $10^{9}\ M_{\odot}$, BH accretion drives a sufficiently energetic wind to clear obscuring material from the central regions of the system and powers an optically luminous quasar similar to J1148+5251. We have devised a set of novel multiscale simulations, which include cosmological *N*-body calculations on large scales and hydrodynamic simulations of galaxy mergers on galactic scales, coupled with the self-regulated growth of SMBHs, enabling us to follow galaxy assembly and quasar formation at $z \sim 6$.

This paper is organized as follows. In § 2 we describe our computational methods and models, which include a set of large-scale cosmological *N*-body simulations and hydrodynamical galaxy mergers along the merging history of the quasar halo. In § 3 we present the formation and evolution of the quasar and its host galaxy, including the assembly of the galaxy progenitors, star formation, and SMBH growth, as well as the SMBH-host correlations and properties of the quasar such as luminosities and lifetimes. We discuss feedback from starburst-driven winds, quasar abundances for cosmological models with different parameters, the implication of BH mergers, and galaxies in the epoch of reionization in § 4, and we summarize in § 5.

2. METHODOLOGY

Rare, high-redshift quasars originate in highly overdense regions in the initial dark matter density distribution and grow through hierarchical mergers, as predicted by the ΛCDM theory. Simulations of high-redshift quasar formation must model a large cosmological volume to accommodate the low abundance of this population, have a large dynamic range to follow the hierarchical buildup of the quasar hosts, and include the hydrodynamics of the gas flows in galaxy mergers. The cutting edge Millennium Simulation by Springel et al. (2005c) follows structure formation in a box with side length of 500 h^{-1} Mpc using 2160^3 dark matter particles. It reproduces the large-scale galaxy distribution as observed (Springel et al. 2006) and identifies an early quasar halo candidate at $z = 6.2$ that ends up in the richest cluster at the present day. However, even such a large dynamic range still falls short of being able to follow the formation and evolution of the rarest quasars observed at the highest redshifts. Moreover, in order to address the properties of quasars and host galaxies, gasdynamics and physical processes related to star formation and BH growth must be included. To satisfy these requirements, we have performed a set of novel multiscale simulations that enable us to resolve individual mergers on galactic scales and retain the context of large-scale structure formation, as well as the evolution of BHs and stars.

First, we perform a coarse dark matter simulation in a volume of 1 h^{-3} Gpc^3 designed to accommodate the low number density of $z \approx 6$ quasars. The largest halo at $z = 0$, within which the descendants of early, luminous quasars are assumed to reside (Springel et al. 2005c), is then selected for resimulation with higher resolution using a multigrid zoom-in technique developed by Gao et al. (2005). The merging history of the largest halo at $z \sim 6$, which has reached a mass of $\sim 5.4 \times 10^{12}\ h^{-1}\ M_\odot$ through seven major (mass ratio <5:1) mergers between redshifts 14.4 and 6.5, is extracted. These major mergers are again resimulated hydrodynamically using galaxy models scaled appropriately for redshift (Robertson et al. 2006b) and adjusted to account for mass accretion through minor mergers. The simulations include prescriptions for star formation (Springel & Hernquist 2003a) and for SMBH growth and feedback (Di Matteo et al. 2005; Springel et al. 2005b), as described below.

2.1. *Code and Parameters*

Our multiscale simulations were performed using the parallel, *N*-body/smoothed particle hydrodynamics (SPH) code GADGET2 developed by Springel (2005), which is well tested in a wide range of applications from large-scale structure formation to star formation. For the computation of gravitational forces, the code uses the "TreePM" method (Xu 1995), which combines a "tree" algorithm (Barnes & Hut 1986) for short-range forces and a Fourier transform particle-mesh (PM) method (Hockney & Eastwood 1981) for long-range forces. The PM method works efficiently in large-scale cosmological simulations, while the tree method provides accurate forces for the large dynamic range of galaxy merger simulations.

GADGET2 implements the entropy-conserving formulation of SPH (Springel & Hernquist 2002) with adaptive particle smoothing, as in Hernquist & Katz (1989). Radiative cooling and heating processes are calculated assuming collisional ionization equilibrium (Katz et al. 1996; Davé et al. 1999). Star formation is modeled in a multiphase ISM, with a rate that follows the Schmidt-Kennicutt Law (Schmidt 1959; Kennicutt 1998). Feedback from supernovae is captured through a multiphase model of the ISM by an effective equation of state (EOS) for star-forming gas (Springel & Hernquist 2003a). A prescription for SMBH growth and feedback is also included, where BHs are represented by collisionless "sink" particles that interact gravitationally with other components and accrete gas from their surroundings. The accretion rate is estimated from the local gas density and sound speed using a spherical Bondi-Hoyle (Bondi & Hoyle 1944; Bondi 1952) model that is limited by the Eddington rate. Feedback from BH accretion is modeled as thermal energy injected into surrounding gas, as described in Springel et al. (2005b) and Di Matteo et al. (2005).

The simulations presented in this paper adopt the ΛCDM model with cosmological parameters chosen according to the first-year *Wilkinson Microwave Anisotropy Probe* data (WMAP1; Spergel et al. 2003), $(\Omega_m, \Omega_b, \Omega_\Lambda, h, n_s, \sigma_8) = (0.3, 0.04, 0.7, 0.7, 1, 0.9)$. Here Ω_m is the total matter density in units of the critical density for closure, $\rho_{\rm crit} = 3H_0^2/(8\pi G)$. Similarly, Ω_b and Ω_Λ denote the densities of baryons and dark energy at the present day. The Hubble constant is parameterized as $H_0 = 100\ h$ km s^{-1} Mpc^{-1}, while σ_8 is the rms linear mass fluctuation within a sphere of radius 8 h^{-1} Mpc extrapolated to $z = 0$. We have also done the same cosmological simulations with *WMAP* third-year results (WMAP3; Spergel et al. 2007), $(\Omega_m, \Omega_b, \Omega_\Lambda, h, n_s, \sigma_8) = (0.236, 0.042, 0.759, 0.732, 0.95, 0.74)$, for comparison.

2.2. *Cosmological Simulations*

The quasars at $z \sim 6$ have an extremely low comoving space density, $n \sim 10^{-9}$ Mpc^{-3}, and are believed to reside in massive dark matter halos with $M \gtrsim 10^{13}\ M_\odot$ (Fan et al. 2003). Cosmological simulations of quasar formation must therefore model a volume of $\sim 1\ h^{-3}$ Gpc^3 to account for the rarity of such objects. However, in order to resolve a $10^{13}\ M_\odot$ halo at $z \sim 6$ in a cosmological simulation with uniform resolution, a dark matter particle mass at least as small as $10^{11}\ h^{-1}\ M_\odot$ and particle numbers of $>10^9$ are required. Tracking the merger history of such halos requires ~2 orders of magnitude higher resolution and would be computationally prohibitive with standard techniques.

We achieve the mass resolution requirements for the merger history of a $10^{13}\ M_\odot$ halo at $z \sim 6$ by means of a two-step resimulation. First, coarse dark matter cosmological simulations are performed to identify a candidate halo for the quasar host. A cubic volume $L_{\rm box} = 1\ h^{-1}$ Gpc on a side is simulated with 400^3 particles, achieving mass and force resolutions of $m_{\rm DM} \sim 1.3 \times 10^{12}\ h^{-1}\ M_\odot$ and $\epsilon \sim 125\ h^{-1}$ kpc (comoving), respectively. To generate the initial conditions, we use the Boltzmann code CMBFAST by Seljak & Zaldarriaga (1996) to compute a linear theory power spectrum for our chosen cosmology. A random realization of the power spectrum is constructed in Fourier space, sampling modes in a sphere up to the Nyquist frequency of the mesh. The particle distribution is evolved forward in time to $z = 0$ from its initial displacement at $z = 30$ determined using the Zel'dovich approximation.

At the end of the simulation, halos are identified using a "friends-of-friends" (FOF) group-finding algorithm (Davis et al. 1985) with a fixed comoving linking length equal to 0.2 times the mean dark matter interparticle separation and a minimum of 32 particles per group (Springel & Hernquist 2003b). The mean overdensity of the groups corresponds approximately to the expected density of virialized halos (Springel et al. 2005c). From the more than 126,000 groups identified in the 1 h^{-3} Gpc^3 volume at $z = 0$, the largest halo with $M(z = 0) \simeq 3.6 \times 10^{15}\ h^{-1}\ M_\odot$ is selected as a candidate halo for modeling the formation of a quasar at $z = 6.5$.

A multigrid technique developed by Gao et al. (2005) and Power et al. (2003) is used to "zoom in" with high resolution on the selected halo region, which has an effective side length of $L_{\rm box} \sim 50\ h^{-1}$ Mpc. Large-scale tidal forces are captured by binning exterior particles into cells according to their distance from the high-resolution region. To ensure proper treatment of small-scale structure, the initial displacements of the high-resolution particles are calculated assuming a higher initial redshift of $z = 69$ and normalized to σ_8 at $z = 0$. The resimulation uses $\approx 350^3$ particles, with $\approx 340^3$ particles inside the high-resolution region. With this technique, the mass resolution increases by almost 4 orders of magnitude to $m_{\rm DM} \sim 2.8 \times 10^8\ h^{-1}\ M_\odot$, while the spatial resolution reaches $\epsilon \sim 5\ h^{-1}$ kpc.

Figure 1 shows snapshots of both the coarse and high-resolution zoom-in runs that locate the quasar halo candidate. In the coarse run, the "cosmic web" is clearly seen, although the distribution appears nearly homogeneous on such large scales. In the zoom-in run, filamentary structures are prominent. Dark matter collapses along the filaments, and the largest halo forms in the deepest potential wells at the intersections of the filaments. The high resolution of the zoom-in run enables the identification of more halos with lower masses both at $z = 0$ and at high redshifts as early as $z \sim 17$, which is sufficient to identify the halo progenitors of the candidate quasar at $z \sim 6$. It appears that the halo progenitor of the largest one at the present day is also the most massive halo at $z \sim 6$, when it reaches a mass of $M \approx 5.4 \times 10^{12}\ h^{-1}\ M_\odot$, making it a plausible candidate for hosting a rare $z \sim 6.4$ quasar.

2.3. *Halo Mass Functions with Different Cosmological Parameters*

The impact that variations in the cosmological parameters can have on large-scale structure formation can be understood from the theoretical mass function of halos, as derived by Press & Schechter (1974) and later developed by Lacey & Cole (1993). The comoving number density dn of halos of mass between M and $M + dM$ can be described as

$$\frac{dn}{dM} = \sqrt{\frac{2}{\pi}}\, \frac{\rho_0}{M^2}\, \frac{\delta_c(z)}{\sigma(M)} \left| \frac{d \ln \sigma}{d \ln M} \right| \exp\left[-\frac{\delta_c(z)^2}{2\sigma^2(M)} \right], \quad (1)$$

where ρ_0 is the local mean mass density, $\delta_c(z)$ is the critical density of collapse at redshift z linearly extrapolated to the present day, and $\sigma(M)$ is the mass variance, which is a function of the power spectrum $P(k)$ with wavenumber k and the window function $w(k)$, $\sigma^2(M) = (1/2\pi^2) \int_0^\infty P(k) w^2(k)\, d^3k$. The abundance of halos depends on the two functions $\sigma(M)$ and $\delta_c(z)$, each of which involves the cosmological parameters, in particular σ_8, Ω_m, and Ω_Λ. These parameters determine the formation epoch of a halo and its mass.

The recently released WMAP3 results (Spergel et al. 2007) have lower values of σ_8, n_s, and Ω_m, compared to WMAP1 (Spergel et al. 2003). The smaller σ_8 from WMAP3 would lower the amplitude of the power spectrum, which in turn reduces $\sigma(M)$. Furthermore, a smaller Ω_m would reduce $\delta_c(z)$ and hence delay halo formation. So, compared to WMAP1, at a given redshift the WMAP3 parameters would yield a lower abundance of halos with mass $M_{\rm halo} \gtrsim M_*$, where M_* is the halo mass corresponding to the characteristic luminosity in the Schechter luminosity function for galaxies (Schechter 1976), while for $M_{\rm halo} < M_*$, it predicts a slightly larger halo abundance.

To test the sensitivity of our model to the new *WMAP* results, we have performed the same set of cosmological simulations with parameters from the WMAP3 measurements (Spergel et al. 2007). We find that indeed the changes implied by the new parameters primarily affect the formation time and the mass of the candidate quasar halo. For the same random phases in the initial conditions, the location of the most massive halo at $z = 0$ remains the same in both the WMAP1 and WMAP3 runs, except that its mass is reduced by a factor of ~ 1.6 for the WMAP3 parameters. Similarly, the mass of the largest halo at $z \approx 6$ is altered by roughly the same factor. Other notable changes include the following: (1) the formation epoch of the first halo is shifted from $z \sim 16.8$ in the WMAP1 run to $z \sim 14.4$ in the WMAP3 run, and (2) the merging history of the largest halo at $z \sim 6$ moves to lower redshifts in the WMAP3 run, but the number of major mergers remains the same.

Figure 2 shows the halo mass functions from different cosmological simulations. The PS mass function (Press & Schechter 1974) and the one corrected to match numerical simulations by Sheth & Tormen (2002; ST) are also shown for comparison. One important feature in this figure is that the coarse runs agree well with the ST mass function but show a larger comoving density at the high-mass end than that predicted by the PS theory. Our results show that the PS formula underestimates the abundance of high-mass halos by nearly an order of magnitude at $z = 0$, and the discrepancy between the PS calculation and numerical simulations becomes larger at higher redshifts, confirming previous findings (e.g., Jenkins et al. 2001; Sheth & Tormen 2002; Springel & Hernquist 2003b; Springel et al. 2005c). This may explain why previous models using the PS formula to study the abundance of luminous quasars, which presumably form in massive halos, underpredicted the number of bright quasars at $z > 5$ (e.g., Efstathiou & Rees 1988). Furthermore, these results also suggest that the commonly used analytical merger tree generated using the PS formula may not be suitable to study quasar formation at high redshifts.

There are two clear "shifts" of the mass function caused by resolution and cosmological parameters. Those from runs with higher resolution extend to higher redshifts, and at the same redshift, the WMAP1 runs produce more massive halos than the WMAP3 ones. As shown in Figure 2, the coarse runs produce mass functions only up to $z \approx 3$ owing to limited mass resolution, while the zoom-in runs can produce quite reasonable mass functions as early as $z \approx 14$. Because the zoom-in runs were deliberately centered on the highest density peak of the 1 h^{-3} Gpc^3 box, they each contain a very massive halo ($M > 10^{15}\ M_\odot$ at $z = 0$) by construction. This explains why the highest mass bin (which contains only one halo in this case) is ~ 2 orders of magnitude larger than the theoretical curves (ST, PS), which apply only to a *random* region that has a much lower density fluctuation.

To summarize, at a given redshift, runs with the WMAP3 parameters yield slightly less massive halos than ones performed with the WMAP1 values. Or, to put it differently, objects in the WMAP3 cosmology will have masses similar to those for WMAP1, but at slightly later times (i.e., lower redshifts). In what follows, we are primarily concerned with investigating the plausibility of forming $z \sim 6$ quasars through the self-regulated growth of SMBHs in hierarchical mergers, rather than precisely reproducing the properties of an individual quasar at a given redshift, such as J1148+5251. Most of our results are therefore based on runs with the WMAP1 parameters, to ease comparison with previous numerical work. If it were firmly established that, e.g., σ_8 is in reality smaller than its WMAP1 value, then a more exact match to a particular quasar could presumably be obtained

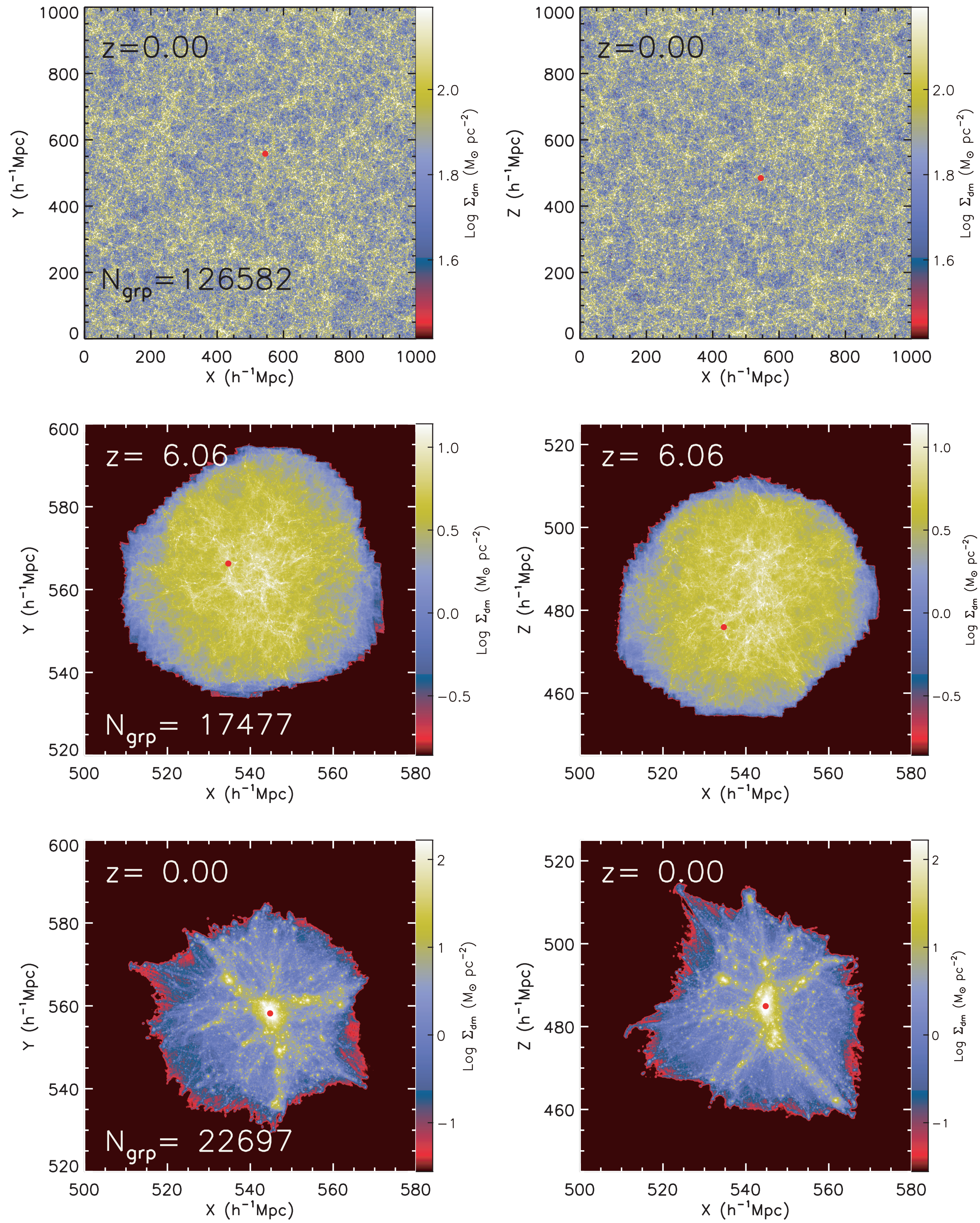

FIG. 1.— Snapshots from a cosmological simulation run with WMAP1 parameters. The images show projected density of dark matter in *x-y* (*left column*) and *x-z* (*right column*) planes; the red dot represents the center of mass of the quasar halo, which is the largest halo at both $z = 0$ and 6. The top panels show the coarse run at $z = 0$. The middle and bottom panels show the zoom-in run at $z = 6.06$ and 0, respectively; the number at the lower left corner indicates the number of groups identified at that redshift.

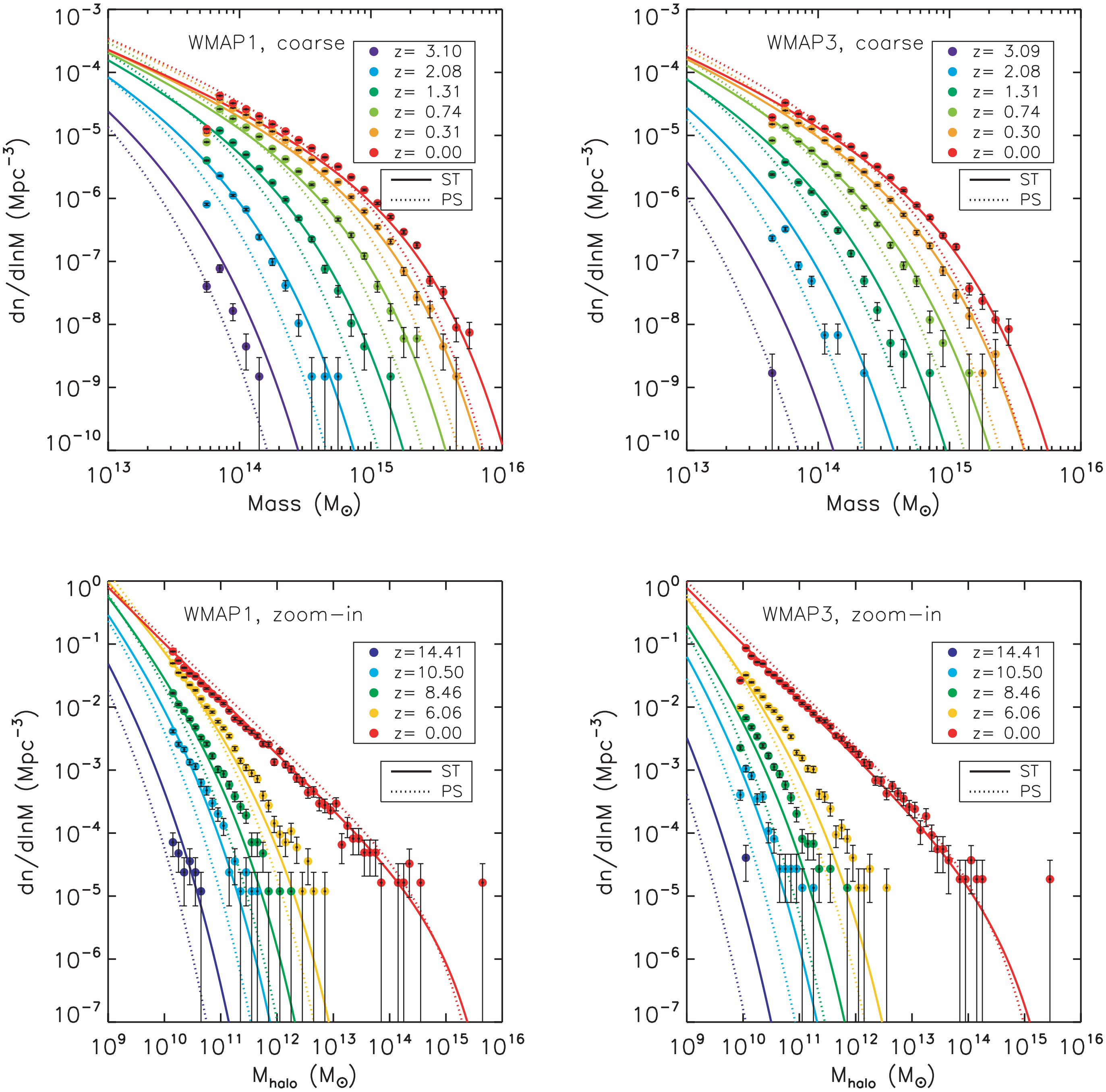

Fig. 2.—Halo mass functions from cosmological simulations with parameters from WMAP1 (*left*) and WMAP3 (*right*) and with different levels of resolution corresponding to our coarse (*top*) and zoom-in (*bottom*) runs. The colored symbols indicate different redshifts, while the error bar shows the Poisson error $\sqrt{N}$. The mass functions from Press & Schechter (1974) (PS; *dotted line*) and Sheth & Tormen (2002) (ST; *solid line*) are also shown for comparison. Please note that in the bottom panels, the analytical curves (ST and PS) apply only to a *random* region; they are not suitable for a highly overdense region where the most massive halos reside in the zoom-in box. Thus, the high-mass end of the simulated mass function deviates significantly from the prediction; see text for more discussion.

by considering larger simulation volumes and identifying a suitable candidate host that is slightly rarer than the one we have chosen to focus on here.

2.4. *Merger Tree Construction*

To follow the hierarchical mass assembly of the host galaxy over cosmic time, the merger tree of the halo is extracted from the cosmological simulation. This tree provides key information for computing the physical properties of the progenitor galaxy population. While the merger history of the halo includes a spectrum of progenitor masses, the most massive progenitors contribute the majority of the halo mass over the redshift range considered. We trace the merger history of the most massive progenitor at each redshift by using particle tags to identify progenitor systems at earlier redshifts in the simulation. Groups that contribute at least 10% of the halo mass at a given time step are considered as the progenitors of the halo and are recorded. The procedure is repeated until the last progenitor is reached, producing the merging history.

Figure 3 illustrates the merging history of the largest halo at $z = 0$ in our cosmological simulation, which has a mass of $\simeq 3.6 \times 10^{15}\ h^{-1}\ M_\odot$. It is also the largest one at $z \sim 6$ with a mass of

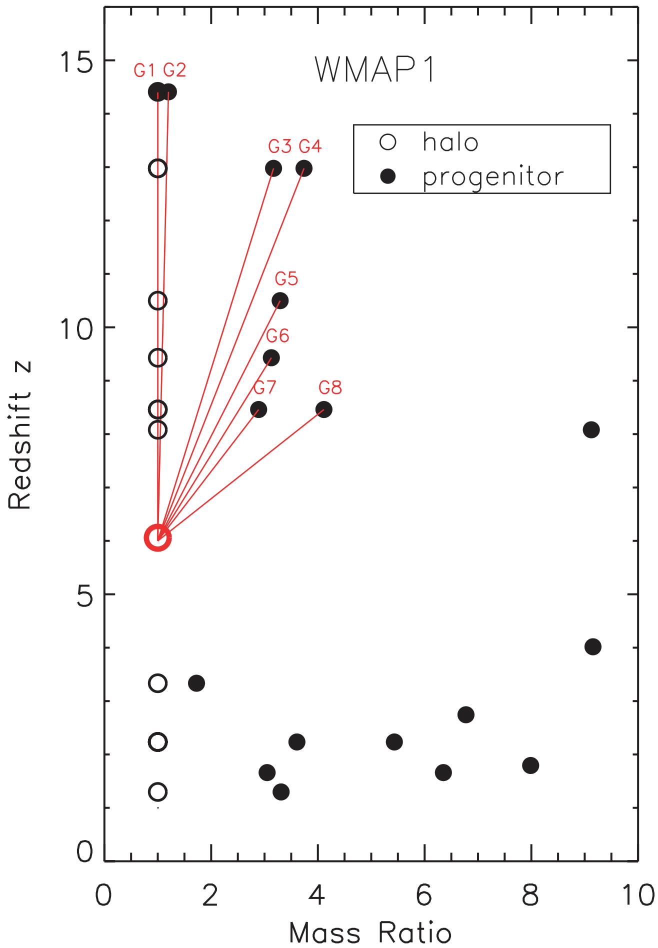

FIG. 3.—Schematic merging history of the largest halo at $z = 0$ traced by mergers at different redshifts with mass ratio $\leq 10:1$, which is defined as the mass ratio between the halo and progenitor at a given time. Each of the progenitors joins in this big merging event at a given redshift, interacts with the system, and subsequently merges with others at later times. The quasar host at $z \sim 6$ is built up by seven successive major mergers of progenitors G1, G2, . . ., G8 from $z \sim 14.4$ to ~ 6.0, as illustrated by the red lines in this plot. The first interaction between G1 and G2 takes place at $z \sim 14.4$, then G3 and G4 join in the system at $z \sim 13$, followed by G5, G6, G7, and G8 at later times (see text for more details). The time line of these events, the mass, and other properties of these progenitors are listed in Table 1.

$\simeq 5.4 \times 10^{12}\ h^{-1}\ M_{\odot}$. This schematic plot outlines the redshift of merger event and the mass ratio of the halo to its galaxy progenitors at a given time. It shows that this halo grows rapidly through hierarchical mergers early on, with seven major mergers (mass ratio of the merging pairs $\leq$5:1) from $z \sim 14.4$ to $\sim$8.5 that build up a substantial fraction of the halo mass at $z \sim 6$.

In modeling the development of a $z \sim 6$ quasar, we are primarily interested in "major" mergers, where the mass ratio of the merging galaxies is not too far from unity, for several reasons. First, it is believed that major mergers play the most important role in the formation and evolution of massive galaxies (e.g., Sanders & Mirabel 1996; Scoville et al. 2000; Veilleux et al. 2002; Conselice et al. 2003; Dasyra et al. 2006). Second, and of greater concern to us in this paper, in our picture for quasar fueling, gas in a rotationally supported disk loses angular momentum through gravitational torques excited by tidal forces in a merger, driving the growth of SMBHs. This process operates most effectively in a major merger because the tidal deformation of each galaxy is significant in such an event (Barnes & Hernquist 1991, 1992, 1996). Collisions involving galaxies with a mass ratio as large as 10 : 1 can induce gas inflows in disks (Hernquist 1989; Hernquist & Mihos 1995), but only for limited orbital configurations. For these reasons, we focus on mergers from the merger tree having a mass ratio $\leq$5:1, as outlined by the red color in Figure 3.

In the resimulation of the merger tree as described in § 2.5, we take into account mass accretion of the halo by adding mass proportionally to each of the eight progenitor galaxies in the major mergers. This approach preserves the progenitor mass ratios and approximately preserves the dynamics of the major mergers (Dubinski 1998).

2.5. *Simulations of Galaxy Mergers along the Tree*

In order to model the formation, evolution, and properties of the quasar candidate, the merger tree is then resimulated hydrodynamically with galaxy models that consist of an extended dark matter halo, a rotationally supported, exponential disk of gas and stars, and a central SMBH. We follow the evolution of the system built up by seven major mergers hierarchically from $z \sim 14.4$ to $\sim$6, as shown in Figure 3. Technically, this is a series of successive merger simulations. The first simulation includes G1 and G2 interacting at $z \sim 14.4$. It stops at $z \sim 13$ and a new galaxy G3 is added into the system. During this process, all the dynamical properties of the preexisting system (e.g., G1 and G2 in this case) are preserved, while G3 is added based on its properties and orbital parameters derived from cosmological simulations. Then a second merger simulation with G1, G2, and G3 starts. Such a procedure is repeated until all the progenitors enter the system. In the end, the simulation includes all eight galaxies. Eventually all these galaxies and BHs merge together. The duration of each merger simulation is determined by the merger tree. The redshift at which each progenitor galaxy enters the merger tree, the properties of each progenitor galaxy, and the numerical parameters of the merger simulations are listed in Table 1. Below we describe the specification of these parameters.

2.5.1. *Galaxy Models*

The structure of the galaxy models is motivated from leading theories of dissipational disk galaxy formation in CDM cosmologies that, as shown by Mo et al. (1998), are successful in reproducing the observed properties of both present-day disk galaxies and damped Lyα absorbers in quasar spectra at high redshift. The initial galaxy models are constructed in dynamical equilibrium using a well-tested method (Hernquist 1993; Springel & White 1999; Springel 2000; Springel et al. 2005b). A halo is identified with a virial mass $M_{\rm vir}$ and a virial radius $R_{\rm vir}$ within which the overdensity $\Delta = \rho_0/\rho_{\rm crit} = 200$, where ρ_0 and $\rho_{\rm crit}$ are the mean and critical density, respectively. The density profile of the dark matter halo follows a Hernquist profile (Hernquist 1990), scaled to match that found in cosmological simulations (Navarro et al. 1997), as described in Springel et al. (2005b):

$$\rho_{\rm Hern}(r) = \frac{M_{\rm vir}}{2\pi} \frac{a}{r(r+a)^3}, \qquad (2)$$

where a is a parameter that relates the Hernquist (1990) profile parameters to the appropriate NFW halo scale length R_s and concentration $C_{\rm vir}$ ($C_{\rm vir} = R_{\rm vir}/R_s$),

$$a = R_s\sqrt{2[\ln(1 + C_{\rm vir}) - C_{\rm vir}/(1 + C_{\rm vir})]}. \qquad (3)$$

The exponential disks of stars and gas are then constructed as in Hernquist (1993) and Springel et al. (2005b). The properties of the galaxy, including the virial mass $M_{\rm vir}$, virial radius $R_{\rm vir}$,

TABLE 1

Progenitor Properties and Numerical Parameters

Galaxy[a]	z[b]	$M_{\rm vir}$[c] (10^{10} h^{-1} $M_\odot$)	$V_{\rm vir}$[d] (km s^{-1})	$f_{\rm gas}$[e]	$M_{\rm BH}$[f] (10^5 h^{-1} $M_\odot$)	R_p[g] (h^{-1} kpc)	R_0[h] (h^{-1} kpc)
G1	14.4	6.3	234.1	1.0	0.15	...	...
G2	14.4	5.3	220.3	1.0	0.15	0.2	7.1
G3	13.0	15.0	297.8	1.0	0.51	0.2	8.5
G4	13.0	17.7	314.6	1.0	0.51	0.3	10.7
G5	10.5	49.1	401.0	1.0	6.56	0.4	11.3
G6	9.4	79.6	448.6	0.9	23.3	0.5	18.2
G7	8.5	160.0	540.4	0.9	89.2	0.7	25.2
G8	8.5	207.7	589.5	0.9	89.2	1.0	34.5

[a] Name of galaxy progenitor. G1 is the halo at $z = 14.4$.
[b] Redshift at which the progenitor enters the merger tree.
[c] Virial mass, assuming overdensity $\Delta = 200$.
[d] Virial velocity, assuming overdensity $\Delta = 200$.
[e] Gas fraction of the progenitor baryonic mass.
[f] Progenitor BH mass at the merger redshift.
[g] Pericentric distance of the incoming progenitor to the center of mass of the existing system.
[h] Initial distance of the incoming progenitor to the existing system.

and halo concentration $C_{\rm vir}$, are scaled appropriately with redshift, as described in Robertson et al. (2006b). In particular, for a progenitor with virial velocity $V_{\rm vir}$ at redshift z, $M_{\rm vir}$ and $R_{\rm vir}$ are calculated following Mo et al. (1998), while $C_{\rm vir}$ is adopted from Bullock et al. (2001) as briefly outlined below:

$$M_{\rm vir} = \frac{V_{\rm vir}^3}{10GH(z)}, \tag{4}$$

$$R_{\rm vir} = \frac{V_{\rm vir}}{10H(z)}, \tag{5}$$

$$H(z) = H_0\left[\Omega_\Lambda + (1-\Omega_\Lambda-\Omega_m)(1+z)^2 + \Omega_m(1+z)^3\right]^{1/2}, \tag{6}$$

$$C_{\rm vir} = 9\left(\frac{M_{\rm vir}}{M_0}\right)^{-0.13}(1+z)^{-1}, \tag{7}$$

where G is the gravitational constant and $M_0 \sim 8\times10^{12}$ h^{-1} $M_\odot$ is the linear collapse mass at the present epoch.

We assume a baryon fraction of $f_b = 0.15$ for these high-redshift galaxies based on the WMAP1 result (Spergel et al. 2003). The gas fraction of each progenitor is extrapolated from the results of semianalytic models of galaxy formation (Somerville et al. 2001), with 100% gas disks at $z \geq 10$ and 90% at $10 > z \gtrsim 8$. The multiphase ISM is envisioned to consist of cold clouds embedded in a hot, tenuous gas in pressure equilibrium. Stars form out of the cold clouds by gravitational instability (Li et al. 2005) with a rate that is proportional to the surface density of the gas (Schmidt 1959; Kennicutt 1998; Li et al. 2006).

In the adopted ISM model for the gas, the EOS is controlled by a parameter $q_{\rm EOS}$ that linearly interpolates between isothermal gas ($q_{\rm EOS} = 0$) and a strongly pressurized multiphase ISM ($q_{\rm EOS} = 1$). This EOS describes the dynamics of star-forming gas, accounts for the consequences of stellar feedback on galactic scales, and enables us to construct equilibrium disk models even with large gas fractions (Robertson et al. 2004; Springel & Hernquist 2005). Supernova feedback is modeled through thermal energy input into surrounding gas and can help evaporate the cold clouds to replenish the hot phase. For the simulation presented here a value of $q_{\rm EOS} = 0.5$ is used, but test simulations using $q_{\rm EOS} = 0.25$–1.0 produce average star formation and BH accretion rates that converge to within 15%.

2.5.2. *Black Hole Accretion and Feedback*

The SMBHs are represented by collisionless "sink" particles. They interact with other particles gravitationally and accrete the gas. Accretion of gas onto the BHs is modeled using a Bondi-Hoyle-Lyttleton parameterization (Bondi 1952; Bondi & Hoyle 1944; Hoyle & Lyttleton 1941), in which the BHs accrete spherically from a stationary, uniform distribution of gas, as described in Di Matteo et al. (2005) and Springel et al. (2005b):

$$\dot{M}_{\rm B} = \frac{4\pi\alpha G^2 M_{\rm BH}^2 \rho}{\left(c_s^2 + v^2\right)^{3/2}}, \tag{8}$$

where $M_{\rm BH}$ is the BH mass, ρ and c_s are the density and sound speed of the gas, respectively, α is a dimensionless parameter of order unity, and v is the velocity of the BH relative to the gas.

We assume that the accretion has an upper limit by the Eddington rate,

$$\dot{M}_{\rm Edd} \equiv \frac{4\pi G M_{\rm BH} m_p}{\epsilon_r \sigma_{\rm T} c}, \tag{9}$$

where m_p is the proton mass, $\sigma_{\rm T}$ is the Thomson cross section, and ϵ_r is the radiative efficiency. The latter determines the conversion efficiency of mass accretion into energy released as radiated luminosity. We adopt a fixed value of $\epsilon_r = 0.1$, which is the mean value for radiatively efficient Shakura & Sunyaev (1973) accretion onto a Schwarzschild BH. In the simulations, the accretion rate is then the minimum of these two rates, $\dot{M}_{\rm BH} = \min(\dot{M}_{\rm Edd}, \dot{M}_{\rm B})$.

The feedback from the BHs is associated with the mass accretion. We assume that a small fraction ($\simeq$5%) of the radiated energy couples to the surrounding gas isotropically as feedback in the form of thermal energy. This fraction is a free parameter, determined by matching the observed $M_{\rm BH}$-σ relation (Di Matteo et al. 2005). For more discussions on this prescription, see Hopkins et al. (2006a). This feedback scheme self-regulates the growth of the BH and has been demonstrated to successfully reproduce many observed properties of elliptical galaxies, as mentioned earlier.

2.5.3. *Black Hole Seeds*

To grow a BH up to $10^9\ M_\odot$ in less than 800 million years, a wide range in seed masses, from 10 to $10^6\ M_\odot$, have been suggested (e.g., Carr et al. 1984; Loeb & Rasio 1994; Bromm & Loeb 2003; Haiman 2004; Yoo & Miralda-Escudé 2004; Volonteri & Rees 2005; Begelman et al. 2006). The formation of the BH seeds remains an open question, and several scenarios have been proposed. In particular, Fryer et al. (2001) show that rapid collapse of massive Population III stars due to pair instability could produce a BH of $\sim 10^2\ M_\odot$; Bromm & Loeb (2003) suggest that hot and dense gas clumps may collapse monolithically to form a massive BH of $\sim 10^6\ M_\odot$ in metal-free galaxies with a virial temperature of 10^4 K; while Begelman et al. (2006) propose that $\sim 20\ M_\odot$ BHs could form by direct collapse of self-gravitating gas due to global instabilities in protogalactic halos and then grow to 10^4–$10^6\ M_\odot$ with super-Eddington accretion. We adopt the picture where BH seeds are the remnants of the first stars (Abel et al. 2002; Bromm & Larson 2004; Tan & McKee 2004; Yoshida et al. 2006; Gao et al. 2007). The remnant BH mass is currently uncertain and widely debated. Recent theory of Population III star formation predicts a mass range of ~ 30–$500\ M_\odot$, but there are two regimes where an SMBH could form, either $\lesssim 100\ M_\odot$ or $\gtrsim 260\ M_\odot$ (Heger et al. 2003; for a recent discussion see also Yoshida et al. 2006). We have tested the seed mass in the range of 100–300 $M_\odot$ and find that the exponential growth of the BHs during the merger makes our results insensitive to the choice in that range. We therefore assume that the BH seed starts with an initial mass of 200 $M_\odot$ after the collapse of the first star at $z = 30$.

These seed BHs then grow in the centers of a $\sim 10^6\ M_\odot$ halo that contains a large amount of high-density primordial gas, as current theories predict that only one star forms per such minihalo. The dense gas in the central region provides abundant fuel for BH accretion. To account for their evolution before the major mergers take place, the BHs are assumed to grow at the Eddington rate until their host galaxies enter the simulated merger tree. Such an approximation is supported by the fact that the Eddington ratio in the simulations depends on the galaxy interaction and strength of the feedback from the BHs. In our simulations, most BHs grow at nearly the Eddington rate in the early stages of a galaxy interaction when the feedback is weak. However, when the interaction and the feedback become stronger, the Eddington ratios fluctuate by orders of magnitude. So a constant accretion rate at the Eddington limit is no longer appropriate, as we show below. Under this assumption, the first progenitor galaxies (G1 and G2) of the quasar host have BH seeds of order $2 \times 10^4\ h^{-1}\ M_\odot$ by the time it enters the merger tree at $z = 14.4$. However, we should emphasize that this assumption serves only as an upper limit of the early growth of the BHs. Our results in the next sections imply that even if all the BH seeds had a uniform mass of $\sim 10^5\ M_\odot$ when they enter the merger tree, it is still possible to build a massive one to $10^9\ M_\odot$ at $z \sim 6.5$ through gas-rich mergers.

In our model, mergers are invoked in the formation of the most massive BHs of $\gtrsim 10^7\ M_\odot$ because that requires large supplies of gas. Early on, however, this may not be necessary to grow the BH seeds from $\sim 100\ M_\odot$ to the $\sim 10^5\ M_\odot$ we start from because the accretion rate is small so other gas fueling could be sufficient. As demonstrated in Hopkins & Hernquist (2006), faint AGNs could be fueled by stochastic accretion of cold gas that does not involve mergers. A similar process could go on in the BH seeds left by the Population III stars at very high redshifts. We should point out that in our simulations, it is necessary for galaxy progenitors in the merger tree to have reasonable massive BH seeds ($\sim 10^5\ M_\odot$) initially in order to build a $10^9\ M_\odot$ BH at $z \sim 6.5$. However, our results are insensitive to specific formation recipes of the seeds. The formation of seed BHs at high redshifts is a challenging problem, and some of the proposed scenarios mentioned above may indeed be necessary to make our seeds. However, currently there is no observation available to test these models.

In the picture we adopt in which the seeds come from the first stars, the early accretion may be complicated by the feedback from the stars. We note that recent studies by Johnson & Bromm (2007), Abel et al. (2007), and Yoshida et al. (2007) show that H II regions form around the first stars and that the halo gas would be photoionized, photoheated, and evacuated by the radiation feedback from the stars. Johnson & Bromm (2007) suggest that such feedback would deplete the gas in the central region and would delay the BH accretion by up to 10^8 yr. However, this destruction effect depends sensitively on the lifetime of these massive stars and, more importantly, on the environment that determines both the gas density profile and gas replenished from inflow of the expelled gas or neighboring halos. In the simulations presented in Johnson & Bromm (2007) the box size is only 100 h^{-1} kpc, too small to contain the large-scale gravitational potential and the large-wavelength density modes that drive gas infall, so the initial gas density is low and the destruction timescale is long in this case. However, the quasar halo in our simulation resides in the highest density peak in a volume of 1 h^{-1} Gpc^3, where the halo potential and gas density, as well we the accretion rate, are much higher (Gao et al. 2007). For a 200 $M_\odot$ BH, the accretion rate at Eddington limit is only $10^{-6}\ M_\odot\ \mathrm{yr}^{-1}$, which corresponds to the Bondi accretion of molecular gas with a typical temperature of ~ 100 K at density $\sim 10^2\ \mathrm{cm}^{-3}$, as implied from equation (8). Such a density requirement is satisfied with the initial conditions of our model. Therefore, the gas reincorporation timescale in our case may be substantially shorter than that estimated in Johnson & Bromm (2007). We will investigate in a future project the growth and evolution of the early BHs after the death of the first stars in such a cosmological environment, using hydroradiation simulations that include both radiative transfer and BH accretion with ultrahigh resolutions.

2.5.4. *Numerical Parameters of Merger Simulations*

The merger tree contains eight galaxies engaging in seven major mergers at different times. For each merger event, the initial orbits of the incoming progenitors are set to be parabolic, consistent with the majority of the major mergers in our cosmological simulation and with previous findings (Khochfar & Burkert 2006). The orientation of each merging galaxy is selected randomly. The initial separation between each merging pair is set to $R_0 = R_{\mathrm{vir}}$, where R_{vir} is the virial radius of the incoming system, while the pericentric distance is chosen as $R_p = 0.5R_d$, where R_d is the radial disk scale length of the incoming system. We have tested different choices of R_p and orientations and found that the impact of these parameters is minor because the orbital properties of the progenitors change rapidly through interactions with the multiple galaxies in the system.

Throughout the merger simulation, the mass and force resolutions are fixed for each particle type, and the total initial particle number of 1.0×10^6 results in particle masses of $m_h = 1.1 \times 10^7\ h^{-1}\ M_\odot$ for the halo and $m_{g,s} = 2.2 \times 10^6\ h^{-1}\ M_\odot$ for both the gas and stars. The gravitational softening lengths are $\epsilon_h = 60\ h^{-1}$ pc for halo particles and $\epsilon_{g,s} = 30\ h^{-1}$ pc for both gas and stars. In the simulations, it is impossible to resolve individual stars, and the accretion radii of some small BHs are underresolved. However, with the subresolution implementation in our models, we can calculate time-averaged rates of star formation and BH accretion from the large-scale properties of the gas, which are well resolved in our simulations. Resolution studies of a single merger (Springel et al. 2005b) with particle numbers from 1.6×10^5 to 1.28×10^7 show that resolution affects some fine structures of the gas and the instantaneous growth rates of stars and BHs, but the time-averaged properties of the system converge to within 20%.

2.5.5. *Halo Escape Velocity*

In a galaxy merger with BHs, the BHs may merge into one, or may be ejected by gravitational recoil in the final stage. Their fate depends on the halo escape velocity $V_{\rm esc}$. If the recoil velocity is larger than $V_{\rm esc}$, then the BH will be kicked out of the halo. We follow Binney & Tremaine (1987) to calculate this important parameter $V_{\rm esc}$. It is defined by

$$V_{\rm esc}(r) = \sqrt{2|\Phi(r)|}, \tag{10}$$

where $\Phi(r)$ is the gravitational potential at a given radius r. Because the halo is spherical, the potentials of different spherical shells add linearly, so $\Phi(r)$ is contributed by two parts, i.e., shells within r $(r' < r)$ and outside $(r' > r)$:

$$\Phi(r) = -4\pi G\left[\frac{1}{r}\int_0^r \rho_{\rm Hern}(r')r'^2\,dr' + \int_r^\infty \rho_{\rm Hern}(r')r'\,dr'\right], \tag{11}$$

where $\rho_{\rm Hern}(r)$ is again the Hernquist (1990) density profile of the dark matter halo as in equation (2).

Figure 4 shows the escape velocities of the halo progenitors G1–G8 in Table 1, as well as two merger remnants at $z \simeq 14$ and $\simeq 6.5$, respectively. The escape velocity depends on the halo mass, redshift, and distance from the halo center. The $V_{\rm esc}$ remains constant in the central region but begins to decline around $0.1R_{\rm vir}$. At the center, $V_{\rm esc} \sim 2.5V_{\rm vir}$, while at the virial radius $R_{\rm vir}$, the escape velocity is comparable to the virial velocity (by a factor of $\sim$1.5). The isolated halo progenitors G1–G8 have a $V_{\rm esc}$ range of $\sim$385–1029 km s^{-1}. The first merger halo at $z \simeq 14$, which has a mass of $1.66 \times 10^{11}\ M_\odot$ as the merger of G1 and G2, has a central escape velocity of $V_{\rm esc} \sim 486$ km s^{-1}, while the final merger halo at $z \simeq 6.5$, which has a mass of $7.7 \times 10^{12}\ M_\odot$, has $V_{\rm esc} \sim 1284$ km s^{-1}. The shaded region indicates the range of the halo escape velocities of the mergers in our simulations. In particular, the escape speed in the halo central region has a range of 486 km s$^{-1} \lesssim V_{\rm esc} \lesssim 1284$ km s^{-1}. This range is important for analysis of BH ejection from gravitational recoil in the BH binaries in §§ 3.4 and 4.2.

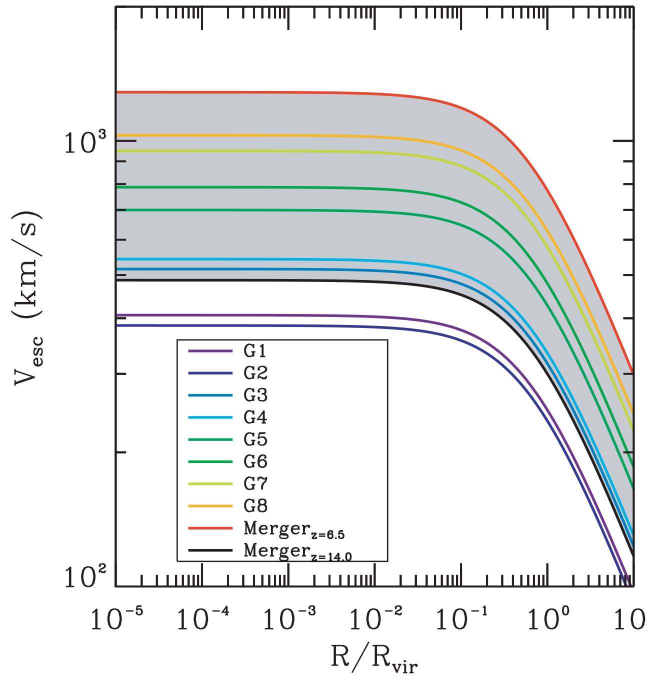

FIG. 4.—Halo escape velocity $V_{\rm esc}$ as a function of distance $R/R_{\rm vir}$ ($R_{\rm vir}$ is the virial radius) to the halo center for various models in our merger simulations. This plot includes the isolated halo progenitors G1–G8 in Table 1, as well as the first merger remnant at $z \simeq 14$ and the last one at $z \simeq 6.5$, as labeled in the legend. The shaded region indicates the range of the escape velocities of the mergers in our simulations, with the values in the central regions being 486 km s$^{-1} \lesssim V_{\rm esc} \lesssim 1284$ km s^{-1}.

3. FORMATION OF A LUMINOUS $z \sim 6$ QUASAR

3.1. *Hierarchical Assembly of the Quasar Host*

The vigorous merging history of the quasar host is illustrated through selected snapshots of the gas and stellar distributions in Figures 5 and 6, respectively. The progenitors at high redshifts are very compact and gas-rich. As the host galaxy of the quasar builds up hierarchically, strong gravitational interactions between the merging galaxies lead to tidal tails, strong shocks, and efficient gas inflow that triggers large-scale starbursts, a phenomenon that has been demonstrated by many numerical simulations (e.g., Hernquist 1989; Hernquist & Katz 1989; Barnes & Hernquist 1991, 1996; Mihos & Hernquist 1994, 1996; Springel 2000; Barnes 2002; Naab & Burkert 2003; Li et al. 2004), as reviewed by Barnes & Hernquist (1992). The highly concentrated gas fuels rapid accretion onto the SMBHs (Di Matteo et al. 2005; Springel et al. 2005b). In the range $z \sim 14$–9, the merging systems are physically small and the interactions occur on the scale of tens of kiloparsecs. By $z \sim 9$–7, when the last major mergers take place, the scale and strength of interactions have increased dramatically. Galaxies are largely disrupted in close encounters, tidal tails of gas and stars extend over hundreds of kiloparsecs, and intense bursts of star formation are triggered.

The BHs continue to grow rapidly during this period but are heavily obscured by a significant amount of circumnuclear gas. During galaxy mergers, the BHs follow their hosts to the center of the system and can interact closely with each other. It has been shown that BH binaries decay rapidly in a gaseous environment and can merge within $\sim 10^7$ yr (Escala et al. 2004; Y. Li 2007, in preparation). Because the galaxies in our simulations are very gas-rich and the gas is highly concentrated during the mergers, we therefore assume that the BHs merge efficiently owing to strong dynamical friction with the gas (Springel et al. 2005b). We discuss this process further in §§ 3.4 and 4.2.

At redshift $z \approx 6.5$ the progenitor galaxies coalesce, inducing high central gas densities that bring the SMBH accretion and feedback to a climax. The SMBH feedback then drives a powerful galactic wind that clears the obscuring material from the center of the system. The largest SMBH becomes visible as an optically bright quasar (Hopkins et al. 2006a) during this phase, after which quasar feedback quenches star formation and self-regulates SMBH accretion. Consequently, both star formation and quasar activity die down, leaving a remnant that reddens rapidly, as illustrated schematically in Figure 6.

3.2. *Star Formation History*

The evolution of the SFRs of each individual galaxy and the total SFR of the whole system are shown in Figure 7 (*top panel*).

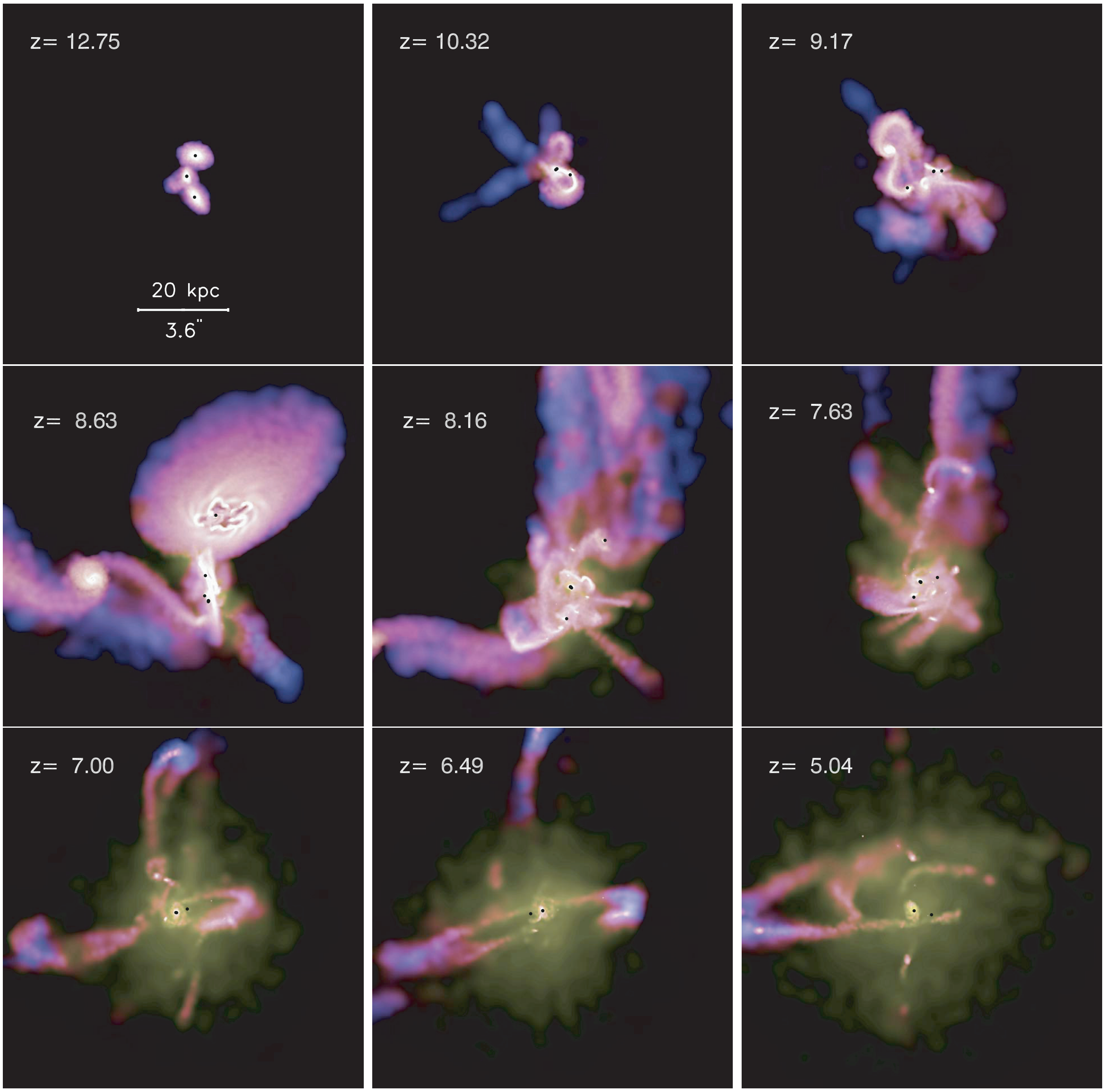

Fig. 5.—History of the quasar host shown in selected snapshots. The images give the projected gas density, color coded by temperature (blue indicates cold gas; yellow indicates hot, tenuous gas). The black dots represent BHs. There are eight galaxies in total, engaging in seven major mergers along the time line of the merger events as listed in Table 1. *Top*: Interactions in the early stage from $z \sim 13$ to 9. *Middle*: Last major mergers between $z \sim 9$ and 7. *Bottom*: Final phase. All the galaxies coalesce at $z \approx 6.5$, creating an extremely luminous, optically visible quasar (see Fig. 6). At this time, there are three BHs, but the luminosity is dominated by the most massive one, which is more than 2 orders of magnitude larger than the others. These BHs merge into a single one at later time. The scale bar indicates a size of 20 kpc (comoving), corresponding to an angular size of 3.6″ at redshift $z = 6.5$.

The system forms stars rapidly as these compact and gas-rich progenitors undergo strong interactions. The total SFR ranges from $\sim$100 to $>10^4\ M_\odot\ \mathrm{yr}^{-1}$ between redshifts $z \sim 9$ and 8 when the galaxies begin their final major mergers, while the SFRs of individual galaxies fall below a few times $10^3\ M_\odot\ \mathrm{yr}^{-1}$, within the starburst intensity limit of $10^3\ M_\odot\ \mathrm{yr}^{-1}\ \mathrm{kpc}^{-2}$ proposed by Meurer et al. (1997) and Thompson et al. (2005). At $z < 7$ the SFR decreases gradually owing to a depletion of the gas supply and progressively stronger feedback from the SMBHs. At the time of final coalescence ($z \approx 6.5$) the SFR is $\sim 100\ M_\odot\ \mathrm{yr}^{-1}$, an order of magnitude lower than for estimates of J1148+5251 (Bertoldi et al. 2003a; Carilli et al. 2004). We note, however, that the estimates by these authors are based on the assumption that the FIR luminosity is dominated by young stars, and they cannot rule out the possibility that AGNs may contribute significantly to the luminosity.

In a forthcoming paper (Li et al. 2007b), we have calculated the infrared properties of the quasar system using a three-dimensional (3D) Monte Carlo radiative transfer code that incorporates adaptive grids and treats dust emission self-consistently. We find that

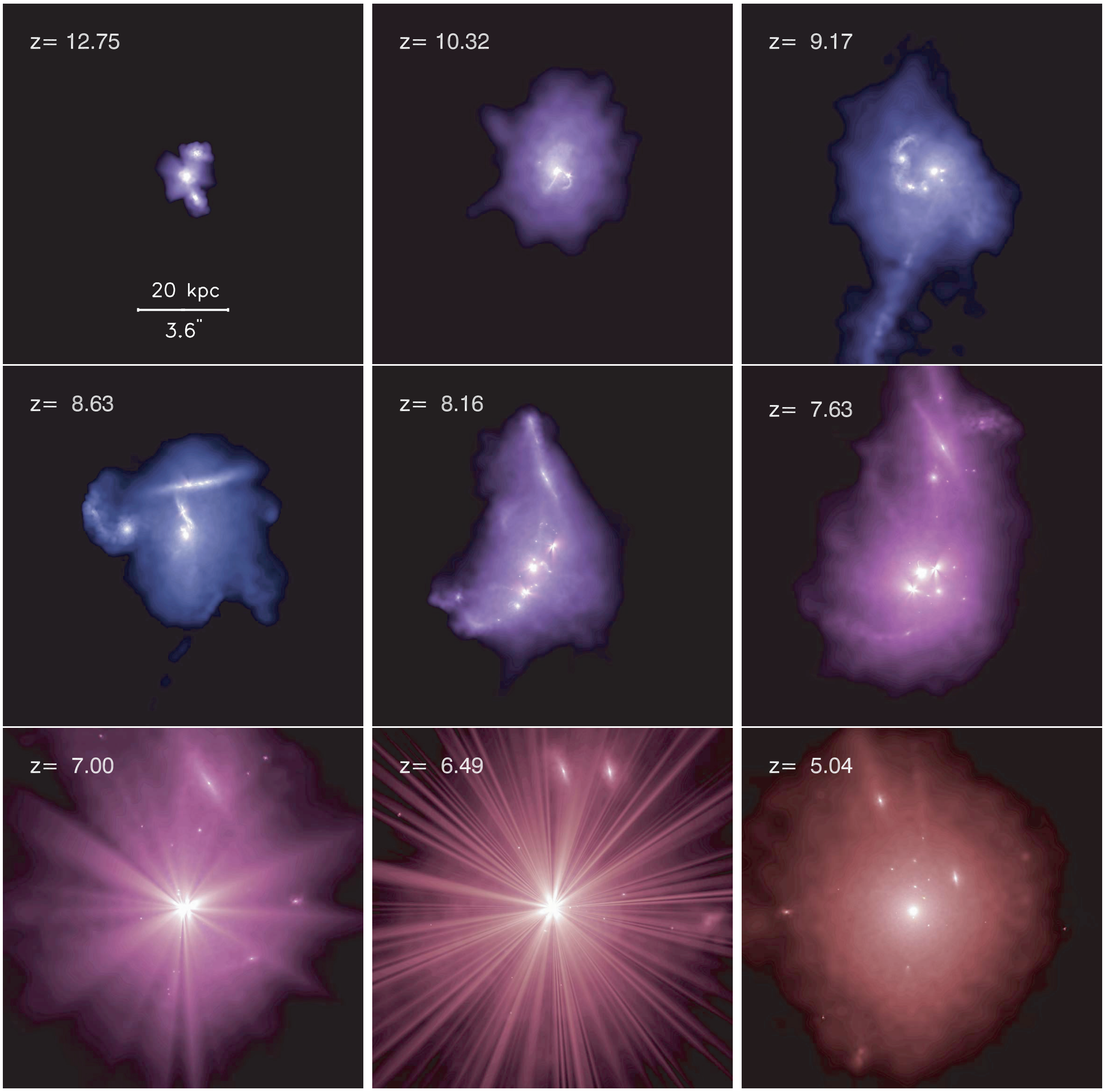

Fig. 6.— Same as Fig. 5, but here the images show the projected stellar density, color coded by the SSFR (SFR per unit stellar mass). Blue indicates massive star formation in the galaxies, while red indicates little star formation. To illustrate the quasar activity, we have generated "rays" around the quasar. The number and strength of the rays are proportional to the bolometric luminosity of the BHs. These rays are artificial and serve only as a visual guide. The systems in the top panels are blue, small, and perturbed. The quasars appear very faint and buried. In the middle panels, strong interactions between galaxies boost star formation and BH accretion, creating highly irregular morphologies and extremely blue galaxies. The quasars are heavily obscured by dense gas. At a later stage (*bottom panels*), feedback from the BHs quenches star formation, allowing the galaxy color to redden. The quasar becomes optically visible as strong outflows blow out the gas. It has a maximum luminosity around $z \approx 6.5$ when all the galaxies coalesce. After that, both the quasar activity and star formation gradually die down, leaving behind an aging stellar spheroid.

the FIR luminosity of our quasar is not dominated by young stars but instead has a substantial quasar contribution of over 80%. This finding is supported by observations of J1148+5251 in NIR (e.g., Charmandaris et al. 2004; Hines et al. 2006; Dwek et al. 2007), which show a remarkably flat SED and suggest an AGN origin for the flux excess. Furthermore, adopting a total gas mass of $\sim 10^{10}\ M_{\odot}$ (Walter et al. 2004; Narayanan et al. 2006c) in J1148+5251, a simple application of the Schmidt-Kennicutt star formation law (Schmidt 1959; Kennicutt 1998) gives an SFR of $\sim 200\ M_{\odot}\ \mathrm{yr}^{-1}$, close to what we find here.

Within only about 600 Myr from $z = 14.4$ to 6.5, the system accumulates a stellar mass of $\sim 10^{12}\ M_{\odot}$ as shown in Figure 7 (*bottom panel*). The specific star formation rate (SSFR), or "*b* parameter" (e.g., Brinchmann et al. 2004), is defined as SSFR = SFR/M_{star}. It is a measure of the fraction of the total stellar mass currently forming at a specific time. The SSFR is typically larger in high-redshift galaxies than in ones at low redshifts owing to vigorous star formation. During the past several years, there has been rapid progress in observing galaxies at $z \gtrsim 6$ using the *Hubble Space Telescope* (*HST*) and the *Spitzer Space Telescope*

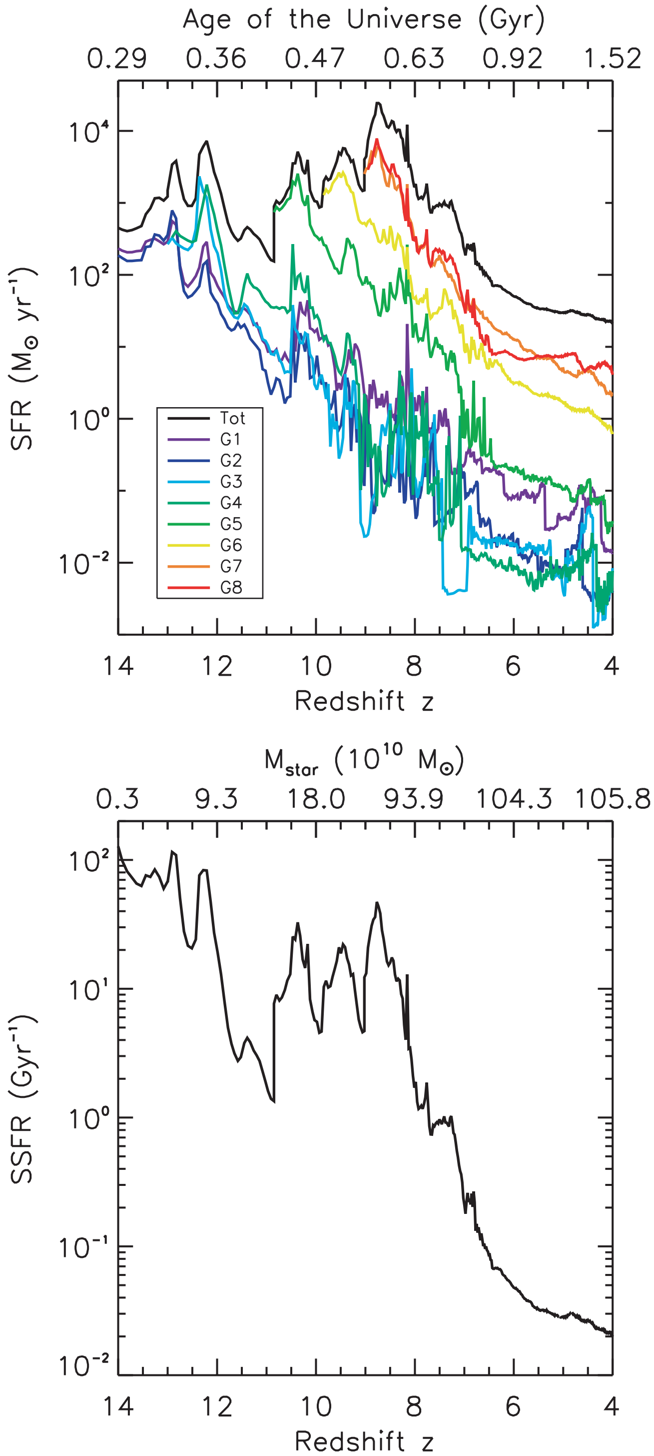

FIG. 7.—Time evolution of SFR (*top*) and SSFR (*bottom*). The colored lines indicate individual galaxies, while the black lines give summed quantities for the entire system.

coupled with ground-based observatories (e.g., Dickinson et al. 2004; Bunker et al. 2004; Bouwens et al. 2004; Giavalisco et al. 2004; Egami et al. 2005; Eyles et al. 2005; Mobasher et al. 2005; Yan et al. 2005, 2006; Eyles et al. 2007), and hundreds of these distant objects have been detected. These frontier observations suggest that the universe experienced rapid star formation during the redshift interval $14 \gtrsim z \gtrsim 6$ and the development of large stellar systems in the mass range of $\sim 10^{10}$–10^{11} $M_\odot$. In particular, several groups (Egami et al. 2005; Yan et al. 2006; Eyles et al. 2007) find SSFRs in the range of 10^{-1} to 10^2 Gyr^{-1} in their observations, consistent with our simulations.

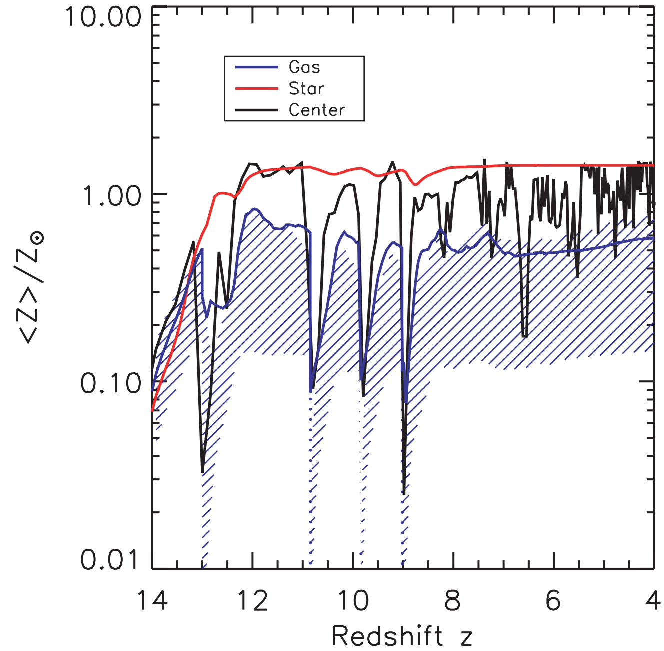

FIG. 8.—Time evolution of mass-weighted metallicity in the quasar host, from gas (*blue line*), stars (*red line*), and the mean value in the central region ($R <$ 1 kpc) of each galaxy (*black line*). The blue hatched region indicates the range of 25%–75% of the gas metallicity.

3.3. *Metal Enrichment*

Rapid star formation in the quasar progenitors produces an abundant mass of heavy elements to enrich the ISM. Observations of J1148+5251 show solar metallicity in the system (Barth et al. 2003; Walter et al. 2003; Maiolino et al. 2005; Becker et al. 2006). Figure 8 shows the metallicity in our simulated quasar system at different times. Note that the dips and jumps in the curves owe to incoming new galaxies that bring in metal-poor pristine gas and newly formed stars. The quasar host reaches solar metallicity as early as $z \sim 12$ and maintains similar levels to later times. The spatial distribution of metallicity from both gas and stars at the peak quasar phase at $z \approx 6.5$ is shown in Figure 9. The metals are widely spread owing to outflow from the quasar feedback and gas infall toward the merger center. The metallicity in the central region of the merger remnant is slightly above the solar value. In some outer regions, because the gas and stars are still falling back to the system center, the infalling material triggers small-scale bursts of star formation. So the metallicity in these blobs appears to be supersolar, as shown in Figure 9.

Calculations of carbon monoxide emission using non-LTE radiative transfer codes (Narayanan et al. 2006a, 2006b) by Narayanan et al. (2006c) show CO luminosities, excitation patterns, and morphologies within the central $\sim$2 kpc of the quasar host center that are consistent with observations of J1148+5251 (Walter et al. 2003, 2004; Bertoldi et al. 2003b). These results were derived using galactic CO abundances and thus support our conclusions that significant metal enrichment takes place early in the quasar host, as a result of strong star formation in the progenitors.

3.4. *Growth of Supermassive Black Holes*

In the simulations, the quasar host at $z \sim 6$ is built up by eight progenitors, each containing a BH in the center. Figure 10 shows the evolution of the BH accretion rate, the Eddington ratio, and

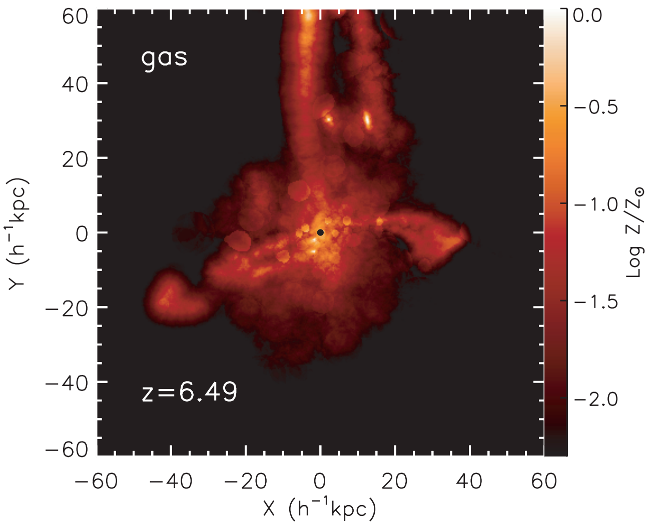

FIG. 9.—Spatial distribution of mass-weighted metallicity of the quasar host at $z \approx 6.5$, from both gas (*top*) and stars (*bottom*). The images are projected metallicity adaptively smoothed over 32 particles (analog to the SPH kernel in a two-dimensional plane). The black dot indicates the center of the quasar.

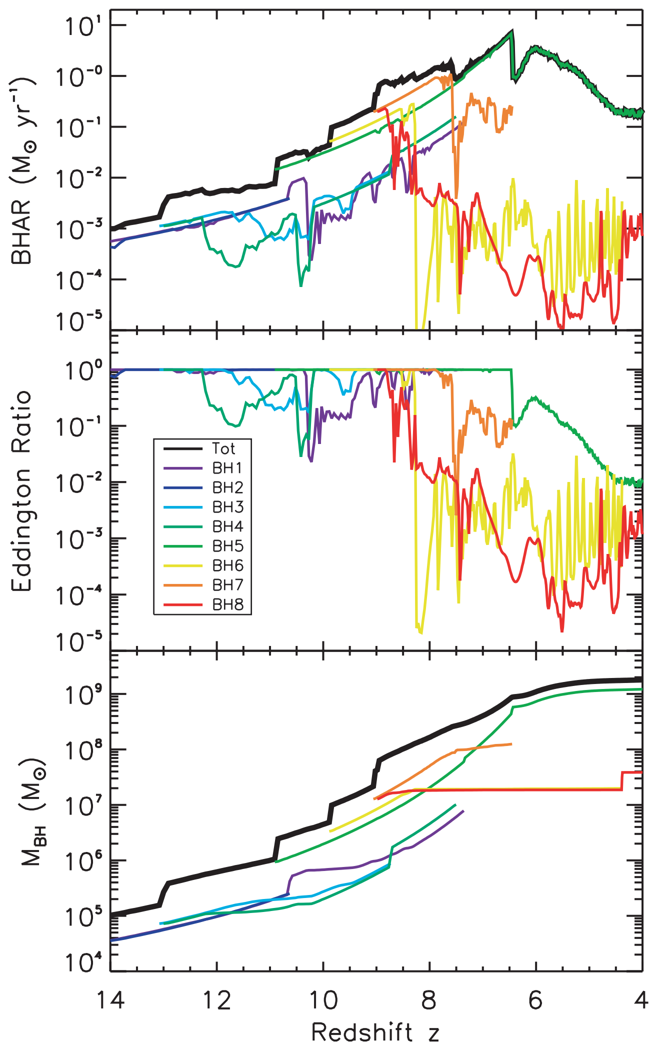

FIG. 10.—Growth history of the quasar system, including the BH accretion rate BHAR (*top*), the Eddington ratio $L_{\rm bol}/L_{\rm Edd}$ (*middle*), and BH mass (*bottom*). Note that the black lines represent totals, while colored lines show individual BHs, as indicated in the legend.

the integrated masses of the whole system and individual BHs. The total BH accretion rate grows steadily during the hierarchical assembly of the host galaxy and peaks at $\sim 10\ M_\odot\ {\rm yr}^{-1}$ around $z \approx 6.5$ during the final coalescence.

The Eddington ratio, $L_{\rm bol}/L_{\rm Edd}$, of each individual BH varies with time, depending on the galaxy interaction and feedback from the BHs. The BHs maintain accretion at the Eddington limit for only a fraction (<50%) of the time. At the peak of quasar activity, the Eddington ratio of the most massive BH is near unity, while that of the other BH is only 0.1. However, collectively, the whole system appears to accrete at $L_{\rm bol}/L_{\rm Edd} \sim 1$ at $z \gtrsim 6.5$, as implied in Figure 10. Studies of BH accretion (e.g., Vestergaard 2004, 2006; Kollmeier et al. 2006) show that the Eddington ratio has a wide range of 0.01–1.0, and it varies with both luminosity and redshift. Luminous systems tend to have higher $L_{\rm bol}/L_{\rm Edd}$ than less luminous counterparts, and at $z \gtrsim 4$, most quasars shine at nearly Eddington luminosity. Our results suggest that *individual* BHs do not always necessarily accrete at the Eddington rate. However, since high-redshift, luminous quasars may form through mergers of several galaxy progenitors containing BHs as in our case, the growth of the quasar therefore represents a *collective* contribution from each individual BH. The total BH mass increases from $\sim 6 \times 10^4\ M_\odot$ at $z \approx 14$ to about $2 \times 10^9\ M_\odot$ at $z \approx 6.5$, close to that estimated for J1148+5251 by Willott et al. (2003) and Barth et al. (2003).

In the simulations, we do have neither sufficient resolution nor the relativistic physics to consider the ejection of BHs by gravitational recoil. The BHs are assumed to merge efficiently once their separation is below the spatial resolution. In the final stage of BH mergers, the emission of the gravitational wave carries linear momentum, which could cause the BHs to recoil (e.g., Bonnor & Rotenberg 1961; Peres 1962). If the recoil velocity is larger than the halo escape velocity, then the BHs will be kicked out from their halo (e.g., Fitchett 1983; Favata et al. 2004; Merritt et al. 2004; Madau & Quataert 2004; Haiman 2004; Yoo & Miralda-Escudé 2004; Volonteri & Rees 2005). Previous studies (Haiman 2004; Yoo & Miralda-Escudé 2004; Volonteri & Rees 2005; Haiman 2006) suggest that constant or super-Eddington accretion is required to produce $10^9\ M_\odot$ BHs at $z \sim 6$ if ejection of BHs is included. In particular, Haiman (2004) suggests that a BH will be ejected if the kick velocity $V_{\rm kick}$ for the coalescing SMBH binary is larger than twice the halo velocity dispersion $\sigma_{\rm halo}$, $V_{\rm kick} \gtrsim 2\sigma_{\rm halo}$, as the dynamical friction timescale for the kicked BH to return to the halo center is longer than the Hubble time (Madau & Quataert 2004). By applying this ejection criterion to a PS merger tree of an $8.5 \times 10^{12}\ M_\odot$ halo within which J1148+5251 is assumed to reside, Haiman (2004) finds that the SMBH of the quasar gains most of its mass rapidly from seed holes during $17 \lesssim z \lesssim 18$ due to BH ejection, and the SMBH likely accretes with a super-Eddington rate in order to build a mass similar to that of J1148+5251.

However, the halo escape velocities or velocity dispersions in our model are much larger than the currently best estimates of the kick velocity. The quasar halo in our simulations has an active merging history from redshifts $z \simeq 14.4$ to $\simeq 6.5$, and the halo progenitors have masses much higher than those considered in the previous studies (Haiman 2004; Yoo & Miralda-Escudé 2004; Volonteri & Rees 2005). The quasar halo builds its mass from $\sim 1.16 \times 10^{11}\ M_\odot$ at $z \simeq 14$ (the sum of progenitors G1 and G2 in Table 1) to $7.7 \times 10^{12}\ M_\odot$ at $z = 6.5$. As shown in Figure 4 (*shaded region*), the central escape velocity of the mergers in our simulations is in the range 486–1284 km s^{-1}. Currently, the maximum kick velocity for unequal-mass, nonrotating BH binaries is in the range of $\sim$74–250 km s^{-1} from both the analytic post-Newtonian approximation (e.g., Blanchet et al. 2005; Damour & Gopakumar 2006) and the groundbreaking full relativistic numerical simulations (e.g., Herrmann et al. 2006; Baker et al. 2006; Gonzalez et al. 2007b). For equal-mass, spinning BH binaries, Favata et al. (2004) estimate a range of $\sim$100–200 km s^{-1} using BH perturbation theory, and Herrmann et al. (2007) derive a formula from relativistic simulations, $V_{\rm kick} = 475S$ km s^{-1}, where $S \leq 1$ is the BH spin. This gives a maximum kick of 475 km s^{-1} for maximal spin, although it is also reported that the recoil velocity can be as large as thousands of kilometers per second (Gonzalez et al. 2007a; Campanelli et al. 2007) for BH binaries in the orbital plane with opposite-directed spin. However, as pointed out by Bogdanovic et al. (2007), such a configuration is rather uncommon, especially in gas-rich galaxy mergers, because torques from accreting gas suffice to align the orbit and spins of both BHs with the large-scale gas flow. The resulting maximum kick velocity from such a configuration is <200 km s^{-1}. Overall, the kick velocity from the latest calculations of BH binaries is in the range of $\sim$100–475 km s^{-1}, falling safely below the escape velocities of the quasar halos in our simulations, so BH ejection may be insignificant in our case.

Moreover, we find that our model can produce a $10^9\ M_\odot$ SMBH even if ejection is allowed. From Figure 10 (*bottom panel*), the $10^9\ M_\odot$ SMBH is dominated by BH5; most of its mass comes from gas accretion. Even if the less massive BHs, for example, BH7 or BH8, were ejected, the most massive one, BH5, is still able to reach $\sim 10^9\ M_\odot$ in the end. Furthermore, even if all the seeds started with $\sim 10^5\ M_\odot$ in the merger tree, the result would be about the same. We therefore conclude that the results from our modeling are robust. SMBHs of $\sim 10^9\ M_\odot$ can grow rapidly through gas accretion and mergers hierarchically in the early universe; constant or super-Eddington accretion is not necessary, unless the recoil velocity of the coalescing BH binary is extremely high such that most of the BH seeds in our simulations are ejected (e.g., $V_{\rm kick} > 1000$ km s^{-1}).

3.5. *Correlations between Supermassive Black Holes and Host Galaxies*

Tight correlations between SMBHs and hosts have been observed in local galaxies (e.g., Magorrian et al. 1998; Ferrarese & Merritt 2000; Gebhardt et al. 2000), but the inference of these relationships at higher redshifts remains an open question. Because the eight galaxies in our system interact vigorously with each other, the stellar components are widely spread and mixed, and it is impossible to separate individual galaxy-SMBH pairs, so we only consider the correlations in the *total* quantity of the whole system. A comparison of the total stellar mass and total BH mass is shown in Figure 11. At early time, both the stars and BHs grow rapidly through galaxy mergers. Shortly after the peak quasar phase, strong feedback suppresses both the accretion and star formation, the masses of the BHs and stars become saturated gradually, and in the end they satisfy $M_{\rm BH} \approx 0.002 M_{\rm star}$, similar to the correlation measured in nearby galaxies (Magorrian et al. 1998; Marconi & Hunt 2003). Our results are consistent with findings by Robertson et al. (2006b) and Hopkins et al. (2007a) and demonstrate that the observed $M_{\rm BH}$-$M_{\rm bulge}$ scaling relation is a result of the coeval growth of the SMBH and its host galaxy and that it holds across different cosmic times.

We note, however, that the velocity dispersion of the stars in the remnant center is about $\sim$500 km s^{-1} (after the system relaxes) owing to the deep potential well of the merger system, so the $M_{\rm BH}$-σ relation falls below the correlation observed locally

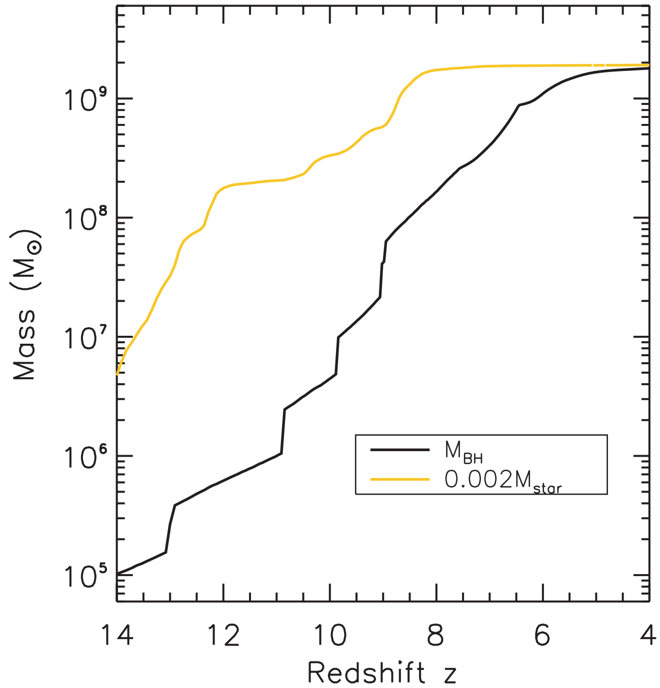

FIG. 11.—Evolution of total BH (*black line*) and stellar (*yellow line*) mass. The stellar mass is multiplied by a factor of 0.002, to reflect the observed correlation of $M_{\rm BH} \approx 0.002 M_{\rm star}$ at the present day, as parameterized by Marconi & Hunt (2003).

(Ferrarese & Merritt 2000; Gebhardt et al. 2000; Tremaine et al. 2002). Single mergers of progenitor galaxies constructed in a redshift range of $z = 0$–6 by Robertson et al. (2006b) appear to follow the observed $M_{\rm BH}$-σ correlation with a weak redshift dependence of the normalization, which results from an increasing velocity dispersion of the progenitors at higher redshift. The multiple mergers we derive from cosmological simulations take place at much higher redshifts and hence the progenitors have larger velocity dispersions, implying a larger deviation from the local $M_{\rm BH}$-σ relation than in the work of Robertson et al. (2006b). However, because we do not follow subsequent mergers and accretion into the host halo below $z \sim 6$, the implications of this result for the evolution of the $M_{\rm BH}$-σ relation are unclear.

Observations of active galaxies have yielded ambiguous results about the SMBH-spheroid relationship. For example, Greene & Ho (2006) report a lower zero point of the $M_{\rm BH}$-σ relation of local active galaxies than that of the inactive sample (Tremaine et al. 2002); at $z > 0$, Shields et al. (2003) found the same $M_{\rm BH}$-σ relation in the redshift range $z = 1$–3, while others (e.g., Treu et al. 2004; Walter et al. 2004; Borys et al. 2005; Peng et al. 2006; Shields et al. 2006) show correlations with various offsets. In particular, Walter et al. (2004) estimate a dynamical mass of $\sim 5 \times 10^{10}\ M_\odot$ using the CO line width measured in J1148+5251 and suggest that the bulge is undermassive by at least 1 order of magnitude compared to the local $M_{\rm BH}$-$M_{\rm bulge}$ relation. However, the CO calculation by Narayanan et al. (2006c) finds that the CO line width of the quasar in our simulation is larger than the mean 280 km s^{-1} measured by Bertoldi et al. (2003b) and Walter et al. (2004) by almost an order of magnitude, and that the derived dynamical mass is $\sim 10^{12}\ M_\odot$, putting the simulated quasar on the $M_{\rm BH}$-$M_{\rm bulge}$ correlation. Narayanan et al. (2006c) further suggest that the observed emission line may be sitting on top of a much broader line, which may be tested by future observations with large bandwidths.

The different relations reported from the observations may reflect a divergence of the methods used to estimate the BH mass and stellar properties, or they may represent different evolutionary stages of the systems (Wu 2007; Hopkins et al. 2007a). More observations and better measurements of BH mass and properties of host bulges will be crucial to study the SMBH-host relations in high-redshift quasar systems (Vestergaard & Peterson 2006) and to test our hypothesis.

3.6. *Quasar Luminosities*

Both the bolometric and attenuated luminosities of the quasar and the host galaxy in the simulations can be readily calculated following the methodology of Hopkins et al. (2005d). The bolometric luminosity $L_{\rm bol}$ of stars is calculated using the stellar population synthesis model of Bruzual & Charlot (2003), while that of a BH is calculated as $L_{\rm bol} = \epsilon_r \dot{M} c^2$, where $\epsilon_r = 0.1$ is the radiative efficiency, $\dot{M}$ is the BH accretion rate, and c is the speed of light. In this calculation, the BHs are assumed to be nonrotating. If the BHs are spinning, their radiative efficiencies and luminosities would be higher due to the shrink of the innermost stable circular orbit, by up to a factor of 4 for maximal rotation.

The *B*-band luminosity of each source is corrected for attenuation by absorption from the ISM along the line of sight. We first calculate the line-of-sight column density of the gas from each source to a distant observer. For each BH we generate 1000 radial sight lines originating at the BH particle location and uniformly spaced in the 4π solid angle $d\cos\theta\, d\phi$, while for the stars, an accurate estimate of the luminosity is possible with only one sight line per source owing to the extended distribution. Along each ray, the gas column density is calculated using a radial spacing of $\Delta r = \eta h_{\rm sml}$, where $\eta \leq 1$ and $h_{\rm sml}$ is the local SPH smoothing length. The distribution of line-of-sight properties converges for $\gtrsim$100 rays and at a distance of $\gtrsim$100 kpc. In the calculation, only the diffuse-phase density is considered because of its large volume filling factor $\geq$99%, allowing for a determination of the lower limit on the column density along a particular line of sight.

Adopting the mean observed intrinsic quasar continuum SED (Richards et al. 2006) gives a *B*-band luminosity that is well approximated by the following equation given by Marconi et al. (2004): $\log(L_{\rm bol}/L_B) = 0.80 - 0.067\mathcal{L} + 0.017\mathcal{L}^2 - 0.0023\mathcal{L}^3$, where $\mathcal{L} = \log(L_{\rm bol}/L_\odot) - 12$ and $\lambda_B = 4400$ Å. We then use the Milky Way gas-to-dust ratio scaled by metallicity, $A_B/N_{\rm H} = (Z/0.02)(A_B/N_{\rm H})_{\rm MW}$, to determine the extinction along a given line of sight for this band. In the above calculation, we do not include a full treatment of radiative transfer and therefore do not model scattering or reprocessing of radiation by dust in the infrared. However, for the *B*-band luminosity, results using a 3D Monte Carlo radiative transfer code are close to those calculated using the methods we present here (Li et al. 2007b; Chakrabarti et al. 2007).

Figure 12 shows both the bolometric and attenuated *B*-band luminosities of the quasar, compared with observations of J1148+5251. The system is intrinsically bright with a total luminosity $>10^{11}\ L_\odot$, and the host appears as an ultraluminous infrared galaxy (ULIRG) with $L_{\rm bol} > 10^{12}\ L_\odot$ for most of the time. At high redshifts, $z > 8$, starlight dominates the total luminosity. However, BHs take over at a later time. The quasar light curve increases dramatically, peaking at $z \approx 6.5$, when it is powered by the most massive BH accreting at near the Eddington rate. The estimated $L_{\rm bol}$ of J1148+5251 differs from that of the simulated quasar by less than the uncertainty in the luminosity estimate. The rest-frame *B*-band absolute magnitude reaches $M_B \sim -26.5$, almost 1 mag fainter than that of J1148+5251 derived from 1450 Å data (Fan et al. 2003). However, we should emphasize that in this

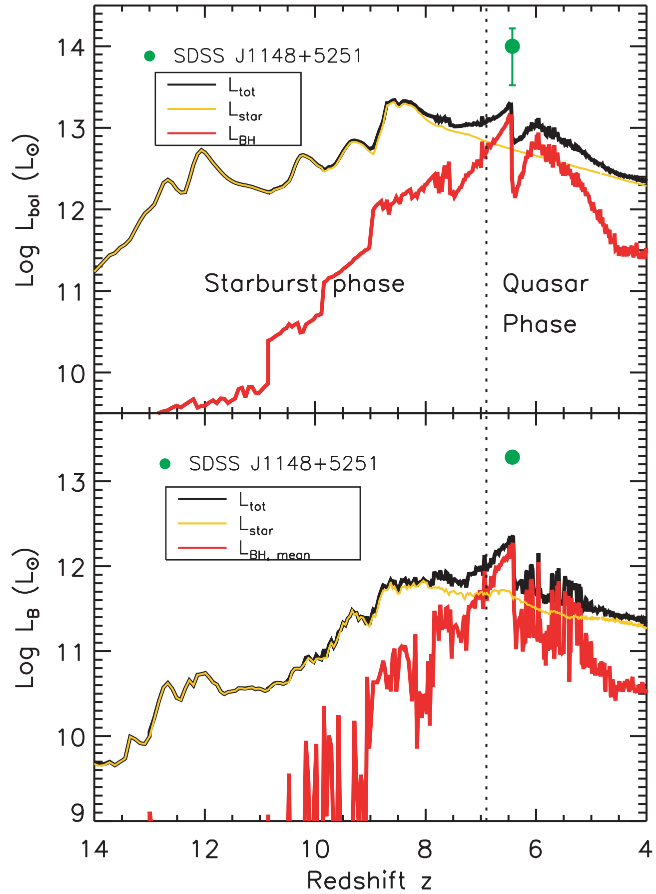

FIG. 12.—Comparison of luminosities from simulations and observations. Shown are bolometric (*top*) and attenuated luminosities in the rest-frame *B* band (*bottom*). Note that $L_{\rm bol}$ of SDSS J1148+5251 (*green filled circle*) is an estimate for an SMBH of $3\times10^9\ M_\odot$ accreting at the Eddington rate, with the error bar indicating the mass range of $(1-5)\times10^9\ M_\odot$ (Willott et al. 2003; Barth et al. 2003), while the L_B is converted from observations at wavelength 1450 Å (Fan et al. 2003). The yellow, red, and black lines represent luminosities of stars, BHs, and total (sum of the above two), respectively. For the BHs, $L_{\rm BH,\,mean}$ is the average luminosity over 1000 sight lines. Note that in the luminosity calculation, the BHs are assumed to be nonrotating. If the BHs are rotating, their radiative luminosities could be higher by up to a factor of a few; see text for more discussions.

paper our main goal is to investigate the plausibility of forming luminous $z \sim 6$ quasars through hierarchical mergers, rather than precisely reproducing the properties of an individual quasar such as J1148+5251, so the disagreement shown in Figure 12 should not be taken too literally. Moreover, the *exact* luminosity can change by a factor of several from relatively trivial or random details in the simulations. If the BH spin is taken into account, then the simulated luminosities would increase by a factor of up to 4, which would match the observation of J1148+5251 better.

Feedback-driven outflows create unobscured lines of sight, allowing the growing central SMBH to be visible as an optically bright quasar between redshifts $z \sim 7.5$ and $\sim$6.4. At the peak of the quasar activity, more than 50% of the 1000 sight lines have $L_B \geq 10^{12}\ L_\odot$. The absorbed light is reemitted at infrared wavelengths by dust. We find that the luminosity in the FIR (Li et al. 2007b) is close to $L_{\rm FIR} \sim 10^{13}\ L_\odot$ estimated for J1148+5251 by Bertoldi et al. (2003a). Moreover, we find that up to 80% of the FIR light comes from the BH, while stars contribute only $\sim$20%. This may explain why the SFR at $z \approx 6.5$ during the peak quasar phase is an order of magnitude lower than the estimate from FIR observations (Bertoldi et al. 2003a), which will be contaminated by the AGN.

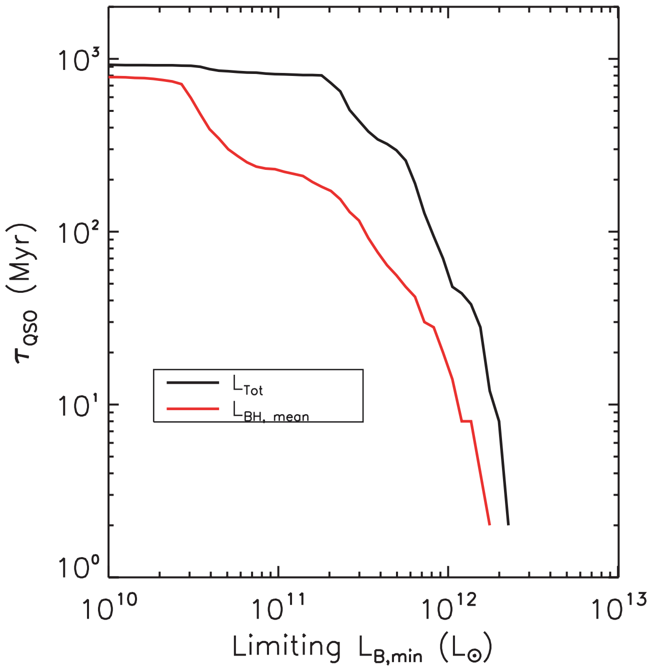

Fig. 13.—Quasar lifetimes as functions of different B-band limiting luminosities. The black and red lines represent the total luminosity of the system and mean luminosity over 1000 sight lines of the BH, respectively, corresponding to the lines of the same color in the bottom panel of Fig. 12.

Another prominent feature of Figure 12 is a clear phase transition from starburst to quasar. It has long been suggested that ULIRGs are powered by starbursts in galaxy mergers (for reviews see Sanders & Mirabel 1996; Jogee 2006) and that bright quasars are the descendants of ULIRGs (Sanders et al. 1988; Norman & Scoville 1988; Scoville 2003; Alexander et al. 2005). This conjecture has been supported by observations of quasar hosts (e.g., Stockton 1978; Heckman et al. 1984; Hutchings & Neff 1992; Bahcall et al. 1997; Hutchings 2005) and theoretical modeling (Hopkins et al. 2006a). In Li et al. (2007b) we calculate the SEDs of the quasar system and its galaxy progenitors. We find that the SEDs of the system at $z > 8$ are characterized by those of starburst galaxies (Sanders & Mirabel 1996), while at the peak quasar phase, the SEDs resemble those observed in $z \sim 6$ quasars (Jiang et al. 2006). We also find that the system evolves from cold to warm ULIRGs as it transforms from starburst to quasar phase. Our results provide further theoretical evidence for the ULIRG-quasar connection in quasar systems in the early universe.

The quasar lifetimes depend on the observed luminosity threshold, as proposed by Hopkins et al. (2005d). In our simulation, at the peak luminosity of $L_B \approx 2 \times 10^{12}\ L_\odot$, the quasar lifetime is roughly $\sim 2 \times 10^6$ yr, as shown in Figure 13. Again, If BH spin is included in the calculation, the luminosity of the quasar would increase by a factor of several, and the quasar lifetime would be longer. However, when increasing the radiative efficiency, the Salpeter time (e-folding time for Eddington-limited BH growth; Salpeter 1964) is increased by an identical factor, meaning that it would also require a longer time to reach the same mass. If high-redshift quasars are rapidly rotating, then our calculations demand either that the seeds be *much* more massive at $z \gtrsim 6$ or that they accrete in a super-Eddington manner. In other words, if the observed Sloan quasars at $z \sim 6$ shine with Eddington luminosity but are rotating rapidly, then our model suggests that their masses would be considerably smaller than estimated.

We note that recent *Spitzer* observations by Jiang et al. (2006) show that 2 out of 13 quasars at $z \sim 6$ have a remarkably low NIR-to-optical flux ratio compared to other quasars at different redshifts, and these authors suggest that the two quasars may have different dust properties. According to our model, however, these two outliers may be young quasars that have just experienced their first major starburst but have not yet reached peak quasar activity, so the light from star formation may be dominant, or comparable to that from the accreting SMBH still buried in dense gas. This may explain the low NIR flux, as well as the B-band luminosity and the narrow Lyα emission line, which are primarily produced by the starburst. We will address this question further in a future paper with detailed modeling and IR calculations (Li et al. 2007b).

4. DISCUSSION

4.1. *Comparison with Previous Models and Robustness of Our Results*

Our multiscale simulations that include large-scale cosmological N-body calculations and hydrodynamic simulations of galaxy mergers, as well as a self-regulated model for BH growth, have successfully produced a luminous quasar at $z \sim 6.5$ with a BH mass of $\sim 2 \times 10^9\ h^{-1}\ M_\odot$ and a number of properties similar to those of J1148+5251, the most distant quasar detected at $z = 6.42$ (Fan et al. 2003). Our approach differs from previous semianalytic studies by Haiman & Loeb (2001), Haiman (2004), Yoo & Miralda-Escudé (2004), and Volonteri & Rees (2005, 2006) in the following ways:

1. We use a realistic merger tree derived directly from multiscale, high-resolution cosmological simulations. The previous studies used merger trees of dark matter halos generated with the extended PS theory (Press & Schechter 1974; Lacey & Cole 1993), which may underestimate the abundance of high-mass halos by up to 1 order of magnitude, as shown in § 2.3. Also, the merger trees in those studies started from much higher redshifts than what we consider here. In our model, the quasar halo is the largest one in a volume of 1 h^{-3} Gpc^3. It has a mass of $\sim 7.7 \times 10^{12}\ M_\odot$ at $z \sim 6.5$ built up through seven major mergers from $z \simeq 14.4$ to $\simeq 6.5$.

2. We follow the evolution of the system and treat the gas dynamics, star formation, and BH growth properly. This approach is critical to investigation of the properties of both BHs and host galaxies and their evolution (e.g., Di Matteo et al. 2005; Springel et al. 2005b; Robertson et al. 2006b; Hopkins et al. 2006a), but it was not included in those previous studies on formation of $z \sim 6$ quasars.

3. We employ a self-regulated model for the growth of SMBHs, in which the accretion is regulated by the BH feedback and the rate is under the Eddington limit. In the previous studies, the BH growth was unregulated, but instead a constant or super-Eddington accretion rate was used.

4. In our simulations, we do not consider BH ejection caused by gravitational recoil owing to insufficient resolution and lack of relativistic physics. However, the halo escape velocities in our simulations are in the range of 486–1284 km s^{-1}, much larger than the kick velocity $\sim$100–475 km s^{-1} (e.g., Herrmann et al. 2006; Baker et al. 2006; Gonzalez et al. 2007b; Herrmann et al. 2007, see §§ 2.5.5 and 3.4 for more details). Therefore, BH ejection may be negligible in our case. Previous studies had much smaller halo progenitors at higher redshifts than ours, so the BH seeds would be more likely subject to ejection from their halos. This leads to the conclusion in these studies that constant or super-Eddington accretion is needed owing to significant BH

ejection. Our results are robust within the best estimates currently available for the recoil velocity of the BH binary.

5. The BH seeds in the galaxy progenitors in our simulations are massive (e.g., $\sim 10^5\ M_\odot$ at $z \sim 14$). The subresolution recipe in our model does not allow us to resolve the actual formation and accretion of such BHs below this mass scale. The formation of these seeds is an unsolved problem, but our results do not depend on the specific prescription of the formation process. We adopt a picture in which the seed holes come from the remnants of the first stars (which have a mass 200 $M_\odot$ at $z = 30$) and grow under the Eddington limit until they enter the merger tree we simulated. If the growth is delayed by radiation feedback from the Population III stars (e.g., Johnson & Bromm 2007), then super-Eddington accretion or other proposed scenarios (e.g., Bromm & Loeb 2003; Begelman et al. 2006) may be necessary to form massive seeds of $\sim 10^5\ M_\odot$ in the protogalaxies.

Overall, we conclude that the results from our simulations, which are more realistic and more detailed than the models previously done, are robust. SMBHs of $\sim 10^9\ M_\odot$ can form rapidly through gas-rich hierarchical mergers under the Eddington limit, even within a short period of time. We find that constant or super-Eddington accretion is not necessary unless the above assumptions in our modeling break, i.e., there are no massive BH seeds of $10^5\ M_\odot$ available at $z \sim 14$, or the recoil velocity of the coalescing BH binary is extremely high (e.g., >1000 km s^{-1}). Under these extreme circumstances, some "exotic" processes such as super-Eddington accretion may be necessary to grow a $\sim 10^9\ M_\odot$ SMBH within a few hundred million years. However, we should note, as pointed out by Bogdanovic et al. (2007), that most gas-rich galaxy mergers have a configuration such that the orbit and spins of both BHs are aligned with the large-scale gas flow owing to torques from accreting gas. Such a configuration has a maximum kick velocity <200 km s^{-1}, which is well below the escape velocity of a $10^{10}\ M_\odot$ dwarf galaxy, as well as those of the halos in our modeling.

4.2. *Merging History of Black Holes*

During the galaxy mergers, the BHs follow their host halos to the system center and can form binaries (or multiple systems). The coalescence of a BH binary includes three distinct phases: inspiral, merger, and ringdown (e.g., Flanagan & Hughes 1998). Whether BH binaries can coalesce on short timescales is a matter of debate. In a stellar environment, it has been argued that a binary hardens very slowly owing to an eventual depletion of stars that cause the binary to lose angular momentum (e.g., Begelman et al. 1980; Milosavljević & Merritt 2003). In a gaseous environment, however, numerical simulations by Escala et al. (2004) and Y. Li (2007, in preparation) show that the binaries decay rapidly owing to strong dynamical friction with the gas, and they likely merge within 10^7 yr. Because our galaxies are very gas-rich and have large central concentrations of gas during the mergers, we assume that the BH particles coalesce once their separation decreases below our spatial resolution (30 h^{-1} pc) and their relative speed falls below the local gas sound speed (Springel et al. 2005b).

In the simulations, we have neither sufficient resolution nor the relativistic physics to consider the ejection of BHs by gravitational recoil during the merger phase. However, as discussed in §§ 2.5.5 and 3.4, the halo escape velocities in our simulations are much larger than the maximum kick velocity for BH binaries estimated from the latest relativistic calculations. So BH ejection is likely unimportant in our modeling. To accurately address gravitational recoil in the galaxy merger simulations, we need to include general relativity, resolve the dynamics of BH binaries with extremely high resolution, and calculate the halo potential in a cosmological context (in which halo potential distribution may be different from that of a single object). However, such a comprehensive treatment is impossible at the moment. We therefore assume that the BHs merge quickly once they reach the stage of gravitational radiation.

These coalescing SMBHs will be strong sources of gravitational radiation detectable by the *Laser Interferometer Space Antenna* (*LISA*; Folkner 1998), as suggested by many authors (e.g., Thorne & Braginskii 1976; Haehnelt 1998; Flanagan & Hughes 1998; Menou et al. 2001; Hughes 2002; Sesana et al. 2005; Koushiappas & Zentner 2006). By tracing the merging history of the SMBHs, *LISA* could shed light on the distribution, structures, and evolution of the associated dark matter halos. Because luminous, high-redshift quasars are likely sites of vigorous hierarchical mergers, they may be the best targets for *LISA* to explore the early universe.

4.3. *Feedback from Starburst-driven Winds*

Vigorous star formation would induce a galactic wind and mass outflow, a phenomenon that has been observed to prevail in both local star-forming galaxies as indicated by blueshifted optical absorption lines (e.g., Martin 1999, 2005; Heckman et al. 2000; Rupke et al. 2002, 2005) and Lyman break galaxies at $z \sim 3$ as indicated by blueshifted interstellar absorption lines and redshifted Lyα emission lines (e.g., Pettini et al. 2002; Shapley et al. 2003), as well as Lyα emitters at $z \sim 5.7$ (Ajiki et al. 2002). These galactic winds are generally thought to play a significant role in galaxy evolution (for recent reviews see, e.g., Veilleux et al. 2005; T. J. Cox et al. 2007, in preparation).

The strong starburst preceding the major quasar phase in our simulations may drive strong galactic winds and affect the BH growth. To investigate the impact of the feedback from a starburst-driven wind on the growth of the BH, we have done the same merger simulation with lower resolution ($N_{\rm tot} \sim 5 \times 10^5$) and with a canonical wind model from Springel & Hernquist (2003b): the wind efficiency $\eta = 0.5$, which measures the coefficient of the star formation that determines the mass outflow; the energy fraction from supernovae injected into the wind $\chi = 0.25$; wind free travel length $L_w = 20$ kpc; and a wind velocity $V_w = 418$ km s^{-1}. As demonstrated by T. J. Cox et al. (2007, in preparation), this wind model is able to reproduce the starbursts as observed in Lyman break galaxies and therefore is suitable to our study.

We find that the impact of the starburst-driven wind on the quasar evolution is minor, as shown in Figure 14. The histories of both star formation and BH growth remain roughly the same as in the simulation without a starburst wind, only the amplitude is lowered by a factor of ~ 1.5. Similarly, the final masses of the BH and the stars are reduced by roughly the same factor, but the quasar host is still on the $M_{\rm BH}$-$M_{\rm bulge}$ correlation. The peak quasar phase is delayed to $z \sim 6$. Overall, the starburst wind affects the gas dynamics locally, but owing to the deep potential of the system, its impact on the process of quasar formation is minor. Our results support the finding by T. J. Cox et al. (2007, in preparation) that feedback from starburst-driven winds alone is ineffective at regulating the growth of the central BH, so feedback from the BH plays the dominant role in the formation and evolution of quasars.

4.4. *Abundance and Fate of Quasar Halos at $z \sim 6$*

Because we have so far simulated only one quasar in a volume of 1 h^{-3} Gpc^3, we are not yet able to constrain the expected

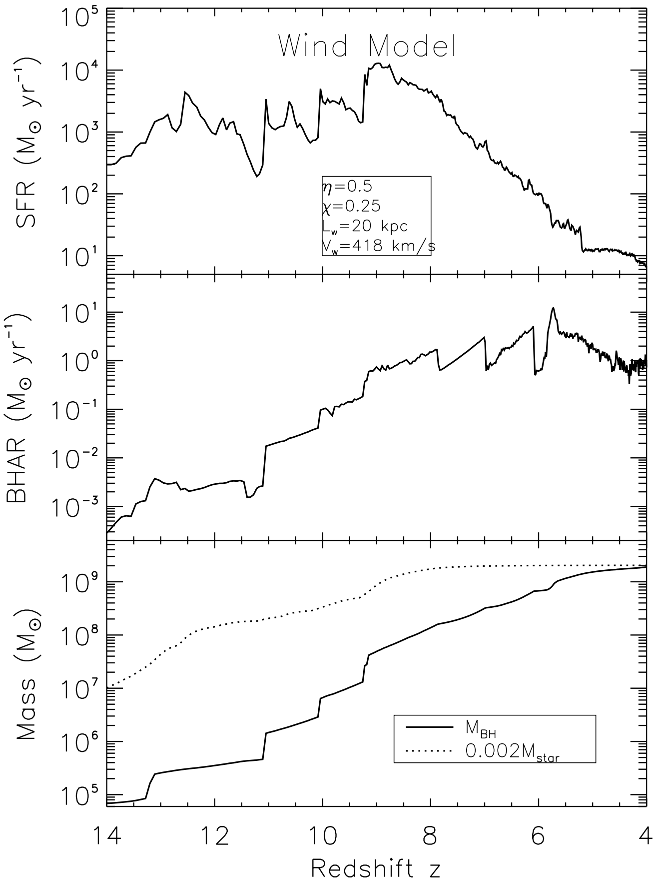

FIG. 14.— Evolution of star formation and BH growth in merger simulations with a starburst-driven wind model. The simulation is run with lower resolution ($N_{\rm tot} \sim 5 \times 10^5$), and the specifications of the wind model are as follows: wind efficiency $\eta = 0.5$, wind energy coefficient $\chi = 0.25$, wind free travel length $L_w = 20$ kpc, and a wind velocity $V_w = 418$ km s^{-1}.

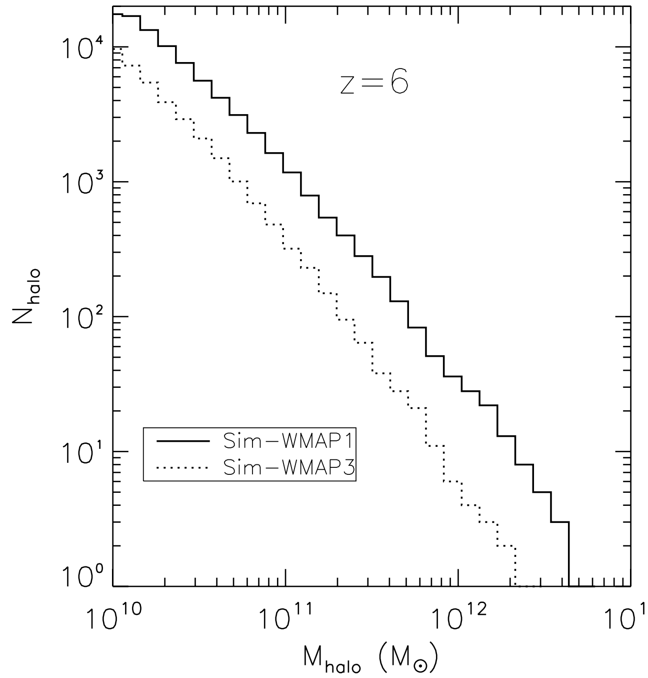

FIG. 15.— Comparison of halo abundances at $z \sim 6$ from the zoom-in simulations with parameters from both WMAP1 (*solid line*) and WMAP3 (*dashed line*). The volume of the high-resolution zoom-in region is $\sim 50^3\ h^{-3}$ Mpc^3.

abundance of quasars at $z \sim 6$. As mentioned in § 2.3, at a given redshift, cosmological simulations with parameters from WMAP1 produce more massive halos than runs with WMAP3 owing to a larger value of σ_8. Figure 15 shows the number of halos at $z \sim 6$ from the zoom-in runs with parameters from both WMAP1 and WMAP3. There are about three dozen halos with mass $M > 10^{12}\ M_\odot$ in the WMAP1 run, while in the WMAP3 run there are only a handful of such halos. However, since in our picture the quasar activity depends not only on the halo mass but also on the merging history, an accurate estimate of the quasar abundance and luminosity function would require hydrodynamical simulations of all the quasar candidates in a large box, which are currently unavailable. Nevertheless, all conditions being equal, the change from the WMAP3 parameters would produce fewer luminous quasars at $z \sim 6$. This suggests that in a WMAP3 cosmology, the quasar observed with the largest redshift, J1148+5251, might have formed in a slightly higher overdensity peak than that we have presented here. In that event, if the WMAP3 determination of σ_8 were correct, we would need to identify a rarer density fluctuation to match J1148+5251 at its observed redshift. However, this does not change our conclusion that the most distant and luminous quasars can form from hierarchical galaxy mergers in the ΛCDM cosmology.

Imaging surveys of J1148+5251 show that there is no other luminous quasar from the same epoch in the field (Carilli et al. 2004; White et al. 2005; Willott et al. 2005). In our simulations, around the peak of quasar activity at $z \approx 6.5$, there are no other halos of mass $>10^{12}\ M_\odot$ within a few Mpc of this quasar. However, the numerous major mergers this halo experienced prior to the peak quasar activity demonstrate that this region was once highly clustered with massive halos, but they merged to become a bigger one by $z = 6.5$.

As seen from Figure 3, this quasar halo will undergo a handful of major mergers at a later time from $z \sim 4$ to 1 and eventually end up as a cD-like galaxy at the center of a rich cluster. Since we do not follow hydrodynamically the evolution of the quasar at $z < 4$, the physical conditions of these mergers remain undetermined. It is not clear whether this halo would experience more episodes of starburst or quasar activity later on during these mergers. Therefore, the final BH mass and other properties of this quasar at the present day are deferred to future simulations that follow its evolution to $z = 0$.

4.5. *Galaxies in the Epoch of Reionization*

The epoch of reionization (EOR) is an important landmark event in cosmic history that constrains the formation of the first luminous objects (Loeb & Barkana 2001). The recent results of WMAP3 indicate that the universe was 50% reionized at $z \approx 9.3$ (Page et al. 2007; Spergel et al. 2007), while studies of Gunn-Peterson absorption (Gunn & Peterson 1965) suggest that reionization began as early as $z \sim 14$ and ended at $z \sim 6$ (Fan et al. 2006). At present, it is believed that the reionization sources are star-forming galaxies since there are insufficient quasars at $z > 6$ as indicated by the steep quasar luminosity function (Fan et al. 2006).

The galaxy progenitors of the quasar in our simulations underwent extreme and prolonged starbursts before $z \sim 6.5$. Less extreme galaxies in this epoch may also have vigorous star formation histories. Detecting these galaxies and determining their contribution to reionization will be crucial to understanding the EOR (Hernquist & Springel 2003; Barton et al. 2004; Davé et al. 2006). As reviewed by Hu & Cowie (2006), recent observations using both broadband colors (e.g., Dickinson et al. 2004; Yan et al. 2005; Bunker et al. 2004; Bouwens et al. 2004; Giavalisco et al. 2004; Egami et al. 2005; Eyles et al. 2005, 2007; Mobasher et al. 2005; Yan et al. 2006) and narrowband Lyα emission (e.g., Hu et al. 2002; Malhotra & Rhoads 2004; Stern et al. 2005) have detected $\sim$500 galaxies at $z \sim 6$ and a handful at $z \gtrsim 7$ (Bouwens et al. 2005). The low-luminosity density of galaxies currently detected at $z > 7$ seems insufficient to reionize the universe. However, ongoing surveys with *HST* and *Spitzer*, as well as future missions such as the Dark Ages z Lyα Explorer (DAzLE; Horton et al. 2004) and the *James Webb Space Telescope* (*JWST*; Windhorst et al. 2006), will search deeper and further for high-redshift objects and may eventually unveil ionizing sources in the EOR.

5. SUMMARY

We have presented a model that accounts for the SMBH growth, quasar activity, and host galaxy properties of the most distant quasar observed at $z = 6.42$, by following the hierarchical assembly of the quasar halo in the standard ΛCDM cosmology. We employ a set of multiscale simulations that include large-scale cosmological *N*-body calculations and hydrodynamic simulations of galaxy mergers and a recipe for BH growth self-regulated by feedback. We first perform a coarse *N*-body simulation in a volume of 1 h^{-3} Gpc^3 to identify the largest halo at $z = 0$, which is assumed to be the descendant of the earliest luminous quasar. We then "zoom in" on the halo and resimulate the region with higher resolution sufficient to extract its merging history starting from very high redshift. The largest halo at $z \sim 6$ reaches a mass of $\sim 5.4 \times 10^{12}\ h^{-1}\ M_\odot$ through seven major mergers between $z \sim 14.4$ and 6.5. These major mergers are again resimulated hydrodynamically using galaxy models and recipes for star formation, SMBH growth, and feedback.

We find that the quasar host galaxy builds up rapidly through gas-rich major mergers, with SFRs up to $10^4\ M_\odot\ \mathrm{yr}^{-1}$, reaching a stellar mass of $\sim 10^{12}\ M_\odot$ at $z \sim 6.5$. The BHs grow through gas accretion under the Eddington limit in a self-regulated manner owing to their own feedback. As the galaxies merge, the BHs coalesce to form a dominant BH, reaching a peak accretion rate of $\sim 20\ M_\odot\ \mathrm{yr}^{-1}$ and a mass of $M_{\mathrm{BH}} \sim 2 \times 10^9\ M_\odot$ at $z \sim 6.5$. Feedback from BH accretion clears away the obscuring gas from the central regions, making the quasar optically visible from $z \sim 7.5$ to 6. At the peak of the quasar phase, the SFR, metallicity, BH mass, and quasar luminosities of the simulated system are consistent with observations of J1148+5251.

Our results demonstrate that rare and luminous quasars at high redshifts can form in the standard ΛCDM cosmology through hierarchical, gas-rich mergers, within the available cosmic time up to the early epoch of $z \approx 6.5$, without requiring exotic processes. Our model should also provide a viable formation mechanism for other distant, luminous quasars. Moreover, we predict that quasar hosts at high redshifts follow a similar M_{BH}-M_{bulge} correlation observed locally as a result of the coeval evolution of the SMBHs and host galaxies. Better measurements of BH masses and host properties with future observations will therefore be crucial to test our prediction. Furthermore, we predict that the progenitors of the distant quasars undergo strong and prolonged starbursts with rates $\sim 10^3\ M_\odot\ \mathrm{yr}^{-1}$ at higher redshifts $z > 8$, which would contribute to the reionization of the universe. Detecting these early galaxies and unveiling the epoch of reionization will be an important goal of current and future missions in observational cosmology.

We thank Volker Bromm, Romeel Davé, Suvendra Dutta, Zoltan Haiman, Scott Hughes, Adam Lidz, Chris McKee, Desika Narayanan, Hans-Walter Rix, Alice Shapley, Rachel Somerville, Curt Struck, Naoshi Sugiyama, Rashid Sunyaev, and Scott Tremaine for stimulating discussions and the referee for helpful comments. Y. L. gratefully acknowledges an Institute for Theory and Computation Fellowship and financial support from the Grants-in-Aid for Young Scientists A17684008 by MEXT (Japan) for a visit to Nagoya. B. R. was supported in part by NASA through the *Spitzer Space Telescope* Fellowship Program through a contract issued by the Jet Propulsion Laboratory, California Institute of Technology, under a contract with NASA. N. Y. acknowledges support from the Grants-in-Aid for Young Scientists A17684008 by MEXT. The computations reported here were performed at the Center for Parallel Astrophysical Computing at Harvard-Smithsonian Center for Astrophysics, while the initial conditions for the cosmological simulations were created on the COSMOLOGY MACHINE supercomputer at the Institute for Computational Cosmology in Durham. This work was supported in part by NSF grant 03-07690 and NASA ATP grant NAG5-13381.

REFERENCES

Abel, T., Bryan, G. L., & Norman, M. L. 2002, Science, 295, 93
Abel, T., Wise, J. H., & Bryan, G. L. 2007, ApJ, 659, L87
Ajiki, M., et al. 2002, ApJ, 576, L25
Alexander, D. M., Smail, I., Bauer, F. E., Chapman, S. C., Blain, A. W., Brandt, W. N., & Ivison, R. J. 2005, Nature, 434, 738
Bahcall, J. N., Kirhakos, S., Saxe, D. H., & Schneider, D. P. 1997, ApJ, 479, 642
Baker, J. G., Centrella, J., Choi, D.-I., Koppitz, M., van Meter, J. R., & Miller, M. C. 2006, ApJ, 653, L93
Barkana, R., & Loeb, A. 2001, Phys. Rep., 349, 125
Barnes, J., & Hut, P. 1986, Nature, 324, 446
Barnes, J. E. 2002, MNRAS, 333, 481
Barnes, J. E., & Hernquist, L. 1992, ARA&A, 30, 705
———. 1996, ApJ, 471, 115
Barnes, J. E., & Hernquist, L. E. 1991, ApJ, 370, L65
Barth, A. J., Martini, P., Nelson, C. H., & Ho, L. C. 2003, ApJ, 594, L95
Barton, E. J., Davé, R., Smith, J.-D. T., Papovich, C., Hernquist, L., & Springel, V. 2004, ApJ, 604, L1
Becker, G. D., Sargent, W. L. W., Rauch, M., & Simcoe, R. A. 2006, ApJ, 640, 69
Becker, R. H., et al. 2001, AJ, 122, 2850
Beelen, A., Cox, P., Benford, D. J., Dowell, C. D., Kovács, A., Bertoldi, F., Omont, A., & Carilli, C. L. 2006, ApJ, 642, 694
Begelman, M. C., Blandford, R. D., & Rees, M. J. 1980, Nature, 287, 307
Begelman, M. C., Volonteri, M., & Rees, M. J. 2006, MNRAS, 370, 289
Bertoldi, F., Carilli, C. L., Cox, P., Fan, X., Strauss, M. A., Beelen, A., Omont, A., & Zylka, R. 2003a, A&A, 406, L55
Bertoldi, F., et al. 2003b, A&A, 409, L47
Binney, J., & Tremaine, S. 1987, Galactic Dynamics (Princeton: Princeton Univ. Press)
Blanchet, L., Qusailah, M. S. S., & Will, C. M. 2005, ApJ, 635, 508
Bogdanovic, T., Reynolds, C. S., & Miller, M. C. 2007, ApJ, 661, L147
Bondi, H. 1952, MNRAS, 112, 195
Bondi, H., & Hoyle, F. 1944, MNRAS, 104, 273
Bonnor, W. B., & Rotenberg, M. A. 1961, Proc. R. Soc. London A, 265, 109
Borys, C., Smail, I., Chapman, S. C., Blain, A. W., Alexander, D. M., & Ivison, R. J. 2005, ApJ, 635, 853
Bouwens, R. J., Illingworth, G. D., Thompson, R. I., & Franx, M. 2005, ApJ, 624, L5
Bouwens, R. J., et al. 2004, ApJ, 606, L25
Brinchmann, J., Charlot, S., White, S. D. M., Tremonti, C., Kauffmann, G., Heckman, T., & Brinkmann, J. 2004, MNRAS, 351, 1151
Bromm, V., & Larson, R. B. 2004, ARA&A, 42, 79
Bromm, V., & Loeb, A. 2003, ApJ, 596, 34
Bruzual, G., & Charlot, S. 2003, MNRAS, 344, 1000
Bullock, J. S., Kolatt, T. S., Sigad, Y., Somerville, R. S., Kravtsov, A. V., Klypin, A. A., Primack, J. R., & Dekel, A. 2001, MNRAS, 321, 559
Bunker, A. J., Stanway, E. R., Ellis, R. S., & McMahon, R. G. 2004, MNRAS, 355, 374
Campanelli, M., Lousto, C. O., Zlochower, Y., & Merritt, D. 2007, ApJ, 659, L5
Carilli, C. L., et al. 2004, AJ, 128, 997
Carr, B. J., Bond, J. R., & Arnett, W. D. 1984, ApJ, 277, 445

Chakrabarti, S., Cox, T. J., Hernquist, L., Hopkins, P. F., Robertson, B., & Di Matteo, T. 2007, ApJ, 658, 840
Charmandaris, V., et al. 2004, ApJS, 154, 142
Conselice, C. J., Bershady, M. A., Dickinson, M., & Papovich, C. 2003, AJ, 126, 1183
Cox, T. J., Di Matteo, T., Hernquist, L., Hopkins, P. F., Robertson, B., & Springel, V. 2006a, ApJ, 643, 692
Cox, T. J., Dutta, S. N., Di Matteo, T., Hernquist, L., Hopkins, P. F., Robertson, B., & Springel, V. 2006b, ApJ, 650, 791
Damour, T., & Gopakumar, A. 2006, Phys. Rev. D, 73, 124006
Dasyra, K. M., et al. 2006, ApJ, 638, 745
Davé, R., Finlator, K., & Oppenheimer, B. D. 2006, MNRAS, 370, 273
Davé, R., Hernquist, L., Katz, N., & Weinberg, D. H. 1999, ApJ, 511, 521
Davis, M., Efstathiou, G., Frenk, C. S., & White, S. D. M. 1985, ApJ, 292, 371
Dickinson, M., et al. 2004, ApJ, 600, L99
Di Matteo, T., Springel, V., & Hernquist, L. 2005, Nature, 433, 604
Djorgovski, S. G., Castro, S., Stern, D., & Mahabal, A. A. 2001, ApJ, 560, L5
Dubinski, J. 1998, ApJ, 502, 141
Dwek, E., Galliano, F., & Jones, A. P. 2007, ApJ, in press
Efstathiou, G., & Rees, M. J. 1988, MNRAS, 230, 5P
Egami, E., et al. 2005, ApJ, 618, L5
Elvis, M., et al. 1994, ApJS, 95, 1
Escala, A., Larson, R. B., Coppi, P. S., & Mardones, D. 2004, ApJ, 607, 765
Eyles, L., Bunker, A., Ellis, R., Lacy, M., Stanway, E., Stark, D., & Chiu, K. 2007, MNRAS, 374, 910
Eyles, L. P., Bunker, A. J., Stanway, E. R., Lacy, M., Ellis, R. S., & Doherty, M. 2005, MNRAS, 364, 443
Fabian, A. C. 1999, MNRAS, 308, L39
Fan, X. 2006, Mem. Soc. Astron. Italiana, 77, 635
Fan, X., Carilli, C. L., & Keating, B. 2006, ARA&A, 44, 415
Fan, X., et al. 2001, AJ, 122, 2833
———. 2003, AJ, 125, 1649
———. 2004, AJ, 128, 515
Favata, M., Hughes, S. A., & Holz, D. E. 2004, ApJ, 607, L5
Ferrarese, L., & Merritt, D. 2000, ApJ, 539, L9
Fitchett, M. J. 1983, MNRAS, 203, 1049
Flanagan, É. É., & Hughes, S. A. 1998, Phys. Rev. D, 57, 4535
Folkner, W. M. 1998, in AIP Conf. Proc. 456, Laser Interferometer Space Antenna, ed. W. M. Folkner (New York: AIP), 11
Fryer, C. L., Woosley, S. E., & Heger, A. 2001, ApJ, 550, 372
Gao, L., Abel, T., Frenk, C. S., Jenkins, A., Springel, V., & Yoshida, N. 2007, MNRAS, in press (astro-ph/0610174)
Gao, L., White, S. D. M., Jenkins, A., Frenk, C. S., & Springel, V. 2005, MNRAS, 363, 379
Gebhardt, K., et al. 2000, ApJ, 539, L13
Giavalisco, M., et al. 2004, ApJ, 600, L103
Glikman, E., Helfand, D. J., & White, R. L. 2006, ApJ, 640, 579
Gonzalez, J. A., Hannam, M. D., Sperhake, U., Brugmann, B., & Husa, S. 2007a, preprint (gr-qc/0702052)
Gonzalez, J. A., Sperhake, U., Bruegmann, B., Hannam, M., & Husa, S. 2007b, Phys. Rev. Lett., 98, 091101
Graham, A. W., Erwin, P., Caon, N., & Trujillo, I. 2001, ApJ, 563, L11
Greene, J. E., & Ho, L. C. 2006, ApJ, 641, L21
Gunn, J. E., & Peterson, B. A. 1965, ApJ, 142, 1633
Haehnelt, M. G. 1998, in AIP Conf. Proc. 456, ed. W. M. Folkner (New York: AIP), 45
Haehnelt, M. G., Natarajan, P., & Rees, M. J. 1998, MNRAS, 300, 817
Haiman, Z. 2004, ApJ, 613, 36
———. 2006, NewA Rev., 50, 672
Haiman, Z., & Loeb, A. 2001, ApJ, 552, 459
Heckman, T. M., Bothun, G. D., Balick, B., & Smith, E. P. 1984, AJ, 89, 958
Heckman, T. M., Lehnert, M. D., Strickland, D. K., & Armus, L. 2000, ApJS, 129, 493
Heger, A., Fryer, C. L., Woosley, S. E., Langer, N., & Hartmann, D. H. 2003, ApJ, 591, 288
Hernquist, L. 1989, Nature, 340, 687
———. 1990, ApJ, 356, 359
———. 1993, ApJS, 86, 389
Hernquist, L., & Katz, N. 1989, ApJS, 70, 419
Hernquist, L., & Mihos, J. C. 1995, ApJ, 448, 41
Hernquist, L., & Springel, V. 2003, MNRAS, 341, 1253
Herrmann, F., Hinder, I., Shoemaker, D., Laguna, P., & Matzner, R. A. 2007, ApJ, 661, 430
Herrmann, F., Shoemaker, D., & Laguna, P. 2006, preprint (gr-qc/0601026)
Hines, D. C., Krause, O., Rieke, G. H., Fan, X., Blaylock, M., & Neugebauer, G. 2006, ApJ, 641, L85
Hockney, R. W., & Eastwood, J. W. 1981, Computer Simulation Using Particles (New York: McGraw-Hill)
Hopkins, P. F., & Hernquist, L. 2006, ApJS, 166, 1
Hopkins, P. F., Hernquist, L., Cox, T. J., Di Matteo, T., Martini, P., Robertson, B., & Springel, V. 2005a, ApJ, 630, 705
Hopkins, P. F., Hernquist, L., Cox, T. J., Di Matteo, T., Robertson, B., & Springel, V. 2005b, ApJ, 630, 716
———. 2005c, ApJ, 632, 81
———. 2006a, ApJS, 163, 1
Hopkins, P. F., Hernquist, L., Cox, T. J., Robertson, B., Di Matteo, T., & Springel, V. 2006b, ApJ, 639, 700
Hopkins, P. F., Hernquist, L., Cox, T. J., Robertson, B., & Krause, E. 2007a, ApJ, submitted (astro-ph/0701351)
Hopkins, P. F., Hernquist, L., Cox, T. J., Robertson, B., & Springel, V. 2006c, ApJS, 163, 50
Hopkins, P. F., Hernquist, L., Martini, P., Cox, T. J., Robertson, B., Di Matteo, T., & Springel, V. 2005d, ApJ, 625, L71
Hopkins, P. F., Richards, G. T., & Hernquist, L. 2007b, ApJ, 654, 731
Hopkins, P. F., Somerville, R. S., Hernquist, L., Cox, T. J., Robertson, B., & Li, Y. 2006d, ApJ, 652, 864
Horton, A., Parry, I., Bland-Hawthorn, J., Cianci, S., King, D., McMahon, R., & Medlen, S. 2004, Proc. SPIE, 5492, 1022
Hoyle, F., & Lyttleton, R. A. 1941, MNRAS, 101, 227
Hu, E. M., & Cowie, L. L. 2006, Nature, 440, 1145
Hu, E. M., Cowie, L. L., McMahon, R. G., Capak, P., Iwamuro, F., Kneib, J.-P., Maihara, T., & Motohara, K. 2002, ApJ, 568, L75
Hughes, S. A. 2002, MNRAS, 331, 805
Hutchings, J. B. 2005, PASP, 117, 1250
Hutchings, J. B., & Neff, S. G. 1992, AJ, 104, 1
Jenkins, A., Frenk, C. S., White, S. D. M., Colberg, J. M., Cole, S., Evrard, A. E., Couchman, H. M. P., & Yoshida, N. 2001, MNRAS, 321, 372
Jiang, L., et al. 2006, AJ, 132, 2127
Jogee, S. 2006, in Physics of Active Galactic Nuclei at all Scales, ed. D. Alloin, R. Johnson, & P. Lira (Berlin: Springer), 143
Johnson, J. L., & Bromm, V. 2007, MNRAS, 374, 1557
Katz, N., Weinberg, D. H., & Hernquist, L. 1996, ApJS, 105, 19
Kazantzidis, S., et al. 2005, ApJ, 623, L67
Kennicutt, R. C., Jr. 1998, ApJ, 498, 541
Khochfar, S., & Burkert, A. 2006, A&A, 445, 403
King, A. 2003, ApJ, 596, L27
Kollmeier, J. A., et al. 2006, ApJ, 648, 128
Koushiappas, S. M., & Zentner, A. R. 2006, ApJ, 639, 7
Lacey, C., & Cole, S. 1993, MNRAS, 262, 627
Li, Y., Haiman, Z., & Mac Low, M.-M. 2007a, ApJ, 663, 61
Li, Y., Hernquist, L., Finkbeiner, D., Fan, X., & Jiang, L. 2007b, ApJ, submitted
Li, Y., Mac Low, M.-M., & Klessen, R. S. 2004, ApJ, 614, L29
———. 2005, ApJ, 620, L19
———. 2006, ApJ, 639, 879
Lidz, A., Hui, L., Zaldarriaga, M., & Scoccimarro, R. 2002, ApJ, 579, 491
Loeb, A., & Barkana, R. 2001, ARA&A, 39, 19
Loeb, A., & Rasio, F. A. 1994, ApJ, 432, 52
Lynden-Bell, D. 1969, Nature, 223, 690
Madau, P., Ferguson, H. C., Dickinson, M. E., Giavalisco, M., Steidel, C. C., & Fruchter, A. 1996, MNRAS, 283, 1388
Madau, P., & Quataert, E. 2004, ApJ, 606, L17
Magorrian, J., et al. 1998, AJ, 115, 2285
Maiolino, R., et al. 2005, A&A, 440, L51
Malhotra, S., & Rhoads, J. E. 2004, ApJ, 617, L5
Marconi, A., & Hunt, L. K. 2003, ApJ, 589, L21
Marconi, A., Risaliti, G., Gilli, R., Hunt, L. K., Maiolino, R., & Salvati, M. 2004, MNRAS, 351, 169
Martin, C. L. 1999, ApJ, 513, 156
———. 2005, ApJ, 621, 227
Menou, K., Haiman, Z., & Narayanan, V. K. 2001, ApJ, 558, 535
Merritt, D., Milosavljević, M., Favata, M., Hughes, S. A., & Holz, D. E. 2004, ApJ, 607, L9
Meurer, G. R., Heckman, T. M., Lehnert, M. D., Leitherer, C., & Lowenthal, J. 1997, AJ, 114, 54
Mihos, J. C., & Hernquist, L. 1994, ApJ, 425, L13
———. 1996, ApJ, 464, 641
Milosavljević, M., & Merritt, D. 2003, ApJ, 596, 860
Mo, H. J., Mao, S., & White, S. D. M. 1998, MNRAS, 295, 319
Mobasher, B., et al. 2005, ApJ, 635, 832
Murray, N., Quataert, E., & Thompson, T. A. 2005, ApJ, 618, 569
Naab, T., & Burkert, A. 2003, ApJ, 597, 893
Narayanan, D., Kulesa, C., Boss, A., & Walker, C. K. 2006a, ApJ, 647, 1426
Narayanan, D., et al. 2006b, ApJ, 642, L107
———. 2006c, ApJ, submitted
Navarro, J. F., Frenk, C. S., & White, S. D. M. 1997, ApJ, 490, 493
Norman, C., & Scoville, N. 1988, ApJ, 332, 124

Page, L., et al. 2007, ApJS, 170, 335
Peng, C. Y., Impey, C. D., Ho, L. C., Barton, E. J., & Rix, H.-W. 2006, ApJ, 640, 114
Peres, A. 1962, Phys. Rev., 128, 2471
Pettini, M., Rix, S. A., Steidel, C. C., Adelberger, K. L., Hunt, M. P., & Shapley, A. E. 2002, ApJ, 569, 742
Power, C., Navarro, J. F., Jenkins, A., Frenk, C. S., White, S. D. M., Springel, V., Stadel, J., & Quinn, T. 2003, MNRAS, 338, 14
Press, W. H., & Schechter, P. 1974, ApJ, 187, 425
Richards, G. T., et al. 2006, ApJS, 166, 470
Robertson, B., Cox, T. J., Hernquist, L., Franx, M., Hopkins, P. F., Martini, P., & Springel, V. 2006a, ApJ, 641, 21
Robertson, B., Hernquist, L., Cox, T. J., Di Matteo, T., Hopkins, P. F., Martini, P., & Springel, V. 2006b, ApJ, 641, 90
Robertson, B., Yoshida, N., Springel, V., & Hernquist, L. 2004, ApJ, 606, 32
Robson, I., Priddey, R. S., Isaak, K. G., & McMahon, R. G. 2004, MNRAS, 351, L29
Rupke, D. S., Veilleux, S., & Sanders, D. B. 2002, ApJ, 570, 588
———. 2005, ApJ, 632, 751
Salpeter, E. E. 1964, ApJ, 140, 796
Sanders, D. B., & Mirabel, I. F. 1996, ARA&A, 34, 749
Sanders, D. B., Soifer, B. T., Elias, J. H., Madore, B. F., Matthews, K., Neugebauer, G., & Scoville, N. Z. 1988, ApJ, 325, 74
Sazonov, S. Y., Ostriker, J. P., Ciotti, L., & Sunyaev, R. A. 2005, MNRAS, 358, 168
Schechter, P. 1976, ApJ, 203, 297
Schmidt, M. 1959, ApJ, 129, 243
Scoville, N. 2003, J. Korean Astron. Soc., 36, 167
Scoville, N. Z., et al. 2000, AJ, 119, 991
Seljak, U., & Zaldarriaga, M. 1996, ApJ, 469, 437
Sesana, A., Haardt, F., Madau, P., & Volonteri, M. 2005, ApJ, 623, 23
Shakura, N. I., & Sunyaev, R. A. 1973, A&A, 24, 337
Shapley, A. E., Steidel, C. C., Pettini, M., & Adelberger, K. L. 2003, ApJ, 588, 65
Shaver, P. A., Wall, J. V., Kellermann, K. I., Jackson, C. A., & Hawkins, M. R. S. 1996, Nature, 384, 439
Sheth, R. K., & Tormen, G. 2002, MNRAS, 329, 61
Shields, G. A., Gebhardt, K., Salviander, S., Wills, B. J., Xie, B., Brotherton, M. S., Yuan, J., & Dietrich, M. 2003, ApJ, 583, 124
Shields, G. A., Menezes, K. L., Massart, C. A., & Vanden Bout, P. 2006, ApJ, 641, 683
Silk, J., & Rees, M. J. 1998, A&A, 331, L1
Sokasian, A., Abel, T., Hernquist, L., & Springel, V. 2003, MNRAS, 344, 607
Somerville, R. S., Primack, J. R., & Faber, S. M. 2001, MNRAS, 320, 504
Songaila, A., & Cowie, L. L. 2002, AJ, 123, 2183
Spergel, D. N., et al. 2003, ApJS, 148, 175
———. 2007, ApJS, 170, 377
Springel, V. 2000, MNRAS, 312, 859
Springel, V. 2005, MNRAS, 364, 1105
Springel, V., Di Matteo, T., & Hernquist, L. 2005a, ApJ, 620, L79
———. 2005b, MNRAS, 361, 776
Springel, V., Frenk, C. S., & White, S. D. M. 2006, Nature, 440, 1137
Springel, V., & Hernquist, L. 2002, MNRAS, 333, 649
———. 2003a, MNRAS, 339, 289
———. 2003b, MNRAS, 339, 312
———. 2005, ApJ, 622, L9
Springel, V., & White, S. D. M. 1999, MNRAS, 307, 162
Springel, V., et al. 2005c, Nature, 435, 629
Stern, D., Yost, S. A., Eckart, M. E., Harrison, F. A., Helfand, D. J., Djorgovski, S. G., Malhotra, S., & Rhoads, J. E. 2005, ApJ, 619, 12
Stockton, A. 1978, ApJ, 223, 747
Tan, J. C., & McKee, C. F. 2004, ApJ, 603, 383
Thompson, T. A., Quataert, E., & Murray, N. 2005, ApJ, 630, 167
Thorne, K. S., & Braginskii, V. B. 1976, ApJ, 204, L1
Tremaine, S., et al. 2002, ApJ, 574, 740
Treu, T., Malkan, M. A., & Blandford, R. D. 2004, ApJ, 615, L97
Veilleux, S., Cecil, G., & Bland-Hawthorn, J. 2005, ARA&A, 43, 769
Veilleux, S., Kim, D.-C., & Sanders, D. B. 2002, ApJS, 143, 315
Vestergaard, M. 2004, ApJ, 601, 676
———. 2006, NewA Rev., 50, 817
Vestergaard, M., & Peterson, B. M. 2006, ApJ, 641, 689
Volonteri, M., & Rees, M. J. 2005, ApJ, 633, 624
———. 2006, ApJ, 650, 669
Walter, F., Carilli, C., Bertoldi, F., Menten, K., Cox, P., Lo, K. Y., Fan, X., & Strauss, M. A. 2004, ApJ, 615, L17
Walter, F., et al. 2003, Nature, 424, 406
White, R. L., Becker, R. H., Fan, X., & Strauss, M. A. 2003, AJ, 126, 1
———. 2005, AJ, 129, 2102
Willott, C. J., McLure, R. J., & Jarvis, M. J. 2003, ApJ, 587, L15
Willott, C. J., Percival, W. J., McLure, R. J., Crampton, D., Hutchings, J. B., Jarvis, M. J., Sawicki, M., & Simard, L. 2005, ApJ, 626, 657
Windhorst, R. A., Cohen, S. H., Jansen, R. A., Conselice, C., & Yan, H. 2006, NewA Rev., 50, 113
Wu, X.-B. 2007, ApJ, 657, 177
Wyithe, J. S. B., & Loeb, A. 2003, ApJ, 595, 614
———. 2005, ApJ, 634, 910
Xu, G. 1995, ApJS, 98, 355
Yan, H., Dickinson, M., Giavalisco, M., Stern, D., Eisenhardt, P. R. M., & Ferguson, H. C. 2006, ApJ, 651, 24
Yan, H., et al. 2005, ApJ, 634, 109
Yoo, J., & Miralda-Escudé, J. 2004, ApJ, 614, L25
York, D. G., et al. 2000, AJ, 120, 1579
Yoshida, N., Oh, S. P., Kitayama, T., & Hernquist, L. 2007, ApJ, 663, 687
Yoshida, N., Omukai, K., Hernquist, L., & Abel, T. 2006, ApJ, 652, 6